Journal of Fluid Mechanics

http://journals.cambridge.org/FLM

Additional services for ***Journal of Fluid Mechanics:***

Email alerts: Click here
Subscriptions: Click here
Commercial reprints: Click here
Terms of use : Click here

Axisymmetric superdirectivity in subsonic jets

André V. G. Cavalieri, Peter Jordan, Tim Colonius and Yves Gervais

Journal of Fluid Mechanics / Volume 704 / August 2012, pp 388 - 420
DOI: 10.1017/jfm.2012.247, Published online: 03 July 2012

Link to this article: http://journals.cambridge.org/abstract_S0022112012002479

How to cite this article:
André V. G. Cavalieri, Peter Jordan, Tim Colonius and Yves Gervais (2012). Axisymmetric superdirectivity in subsonic jets. Journal of Fluid Mechanics,704, pp 388-420 doi:10.1017/jfm.2012.247

Request Permissions : Click here

CAMBRIDGE JOURNALS

Downloaded from http://journals.cambridge.org/FLM, IP address: 131.215.220.186 on 17 Aug 2012

J. Fluid Mech. (2012), *vol.* 704, *pp.* 388–420. © Cambridge University Press 2012
doi:10.1017/jfm.2012.247

Axisymmetric superdirectivity in subsonic jets

André V. G. Cavalieri[1,2]†, Peter Jordan[1], Tim Colonius[3] and Yves Gervais[1]

[1] Département Fluides, Thermique, Combustion, Institut Pprime, CNRS–Université de Poitiers–ENSMA, 86036 Poitiers CEDEX, Poitiers, France

[2] Divisão de Engenharia Aeronáutica, Instituto Tecnológico de Aeronáutica, 12228-900 São José dos Campos, SP, Brazil

[3] Division of Engineering and Applied Science, California Institute of Technology, Pasadena, CA 91125, USA

(Received 7 October 2011; revised 12 April 2012; accepted 23 May 2012; first published online 3 July 2012)

We present experimental results for the acoustic field of jets with Mach numbers between 0.35 and 0.6. An azimuthal ring array of six microphones, whose polar angle, θ, was progressively varied, allows the decomposition of the acoustic pressure into azimuthal Fourier modes. In agreement with past observations, the sound field for low polar angles (measured with respect to the jet axis) is found to be dominated by the axisymmetric mode, particularly at the peak Strouhal number. The axisymmetric mode of the acoustic field can be clearly associated with an axially non-compact source, in the form of a wavepacket: the sound pressure level for peak frequencies is found be superdirective for all Mach numbers considered, with exponential decay as a function of $(1 - M_c \cos\theta)^2$, where M_c is the Mach number based on the phase velocity U_c of the convected wave. While the mode $m = 1$ spectrum scales with Strouhal number, suggesting that its energy content is associated with turbulence scales, the axisymmetric mode scales with Helmholtz number – the ratio between source length scale and acoustic wavelength. The axisymmetric radiation has a stronger velocity dependence than the higher-order azimuthal modes, again in agreement with predictions of wavepacket models. We estimate the axial extent of the source of the axisymmetric component of the sound field to be of the order of six to eight jet diameters. This estimate is obtained in two different ways, using, respectively, the directivity shape and the velocity exponent of the sound radiation. The analysis furthermore shows that compressibility plays a significant role in the wavepacket dynamics, even at this low Mach number. Velocity fluctuations on the jet centreline are reduced as the Mach number is increased, an effect that must be accounted for in order to obtain a correct estimation of the velocity dependence of sound radiation. Finally, the higher-order azimuthal modes of the sound field are considered, and a model for the low-angle sound radiation by helical wavepackets is developed. The measured sound for azimuthal modes 1 and 2 at low Strouhal numbers is seen to correspond closely to the predicted directivity shapes.

Key words: aeroacoustics, jet noise, hydrodynamic noise

† Email address for correspondence: andre.cavalieri@univ-poitiers.fr

1. Introduction

Sound generation by subsonic turbulent jets is a problem comprising coupling between the turbulent motions of the jet and the less complex acoustic motions of the sound field. A difference in complexity is apparent in both the structure of the equations that model the two different kinds of motion, and in the experimentally measured fluctuations in the near and far fields.

If we consider, for instance, the azimuthal dependence of the fluctuations in each region, considerably fewer azimuthal Fourier modes are necessary to represent the sound field than are needed to represent the turbulence (Michalke & Fuchs 1975; Fuchs & Michel 1978). Many researchers have interpreted this low-order azimuthal structure of the sound field as evidence of a corresponding low-order sound-producing turbulence structure (see for instance Crow & Champagne 1971; Moore 1977; Juvé, Sunyach & Comte-Bellot 1979; Hussain & Zaman 1981; Brown & Bridges 2006; Tinney & Jordan 2008).

A candidate source model for the coherent structures is an axially extensive wavepacket. This model can be motivated theoretically by linear stability theory applied to a steady jet base flow, and physically justified by means of a scale-separation argument. The acoustically important features of the wavepacket are its frequency, wavelength, axial amplification, saturation and downstream decay; the saturation is not necessarily associated with nonlinearity, and can be accounted for in a linear framework by appealing to the slow spread of the mean flow (Gudmundsson & Colonius 2011). While Mollo-Christensen (1963, 1967) observed and discussed these features from the point of view of both hydrodynamic stability theory and aeroacoustics, Crow (1972) (see also Crighton 1975) was first to propose a source model, using the framework of Lighthill's (1952) acoustic analogy. The radiation of such sources, for subsonic convection speeds, is highly directive and concentrated at low polar angles θ (measured with respect to the downstream jet axis).

Similar studies were undertaken by Crighton & Huerre (1990), who evaluated the directivity pattern of different envelope functions for the convected wave, and by Sandham, Morfey & Hu (2006), who showed that temporal modulation of such convected wavepackets can further enhance sound radiation. Other variants, proposed by Ffowcs Williams & Kempton (1978) and Cavalieri *et al.* (2011*b*), allow inclusion of the intermittency that is observed in high-Reynolds-number turbulent jets, i.e. the appearance and disappearance of the trains of turbulent 'puffs' observed by Crow & Champagne (1971).

All of the above models have in common their directivity: sound radiation is concentrated at low polar angles with exponential decay at higher polar angles. The term *superdirectivity* was used by Crighton & Huerre (1990) to describe this characteristic of the sound field, and they showed that acoustic non-compactness is a requirement for such radiation.

Experimentally, there is not, for the moment, a complete consensus regarding the relationship between the superdirectivity of wavepacket models and the sound field of subsonic jets; while the latter does present higher sound intensities at low polar angles, it does not have exponential decay as a function of θ. Superdirectivity has been observed in a forced jet by Laufer & Yen (1983), where forcing was effected at a Strouhal number, based on the momentum thickness, of $St_{\delta 2} = 0.017$. The excited jet comprised subharmonics of the forcing frequency, and the directivity of the subharmonic sound radiation was observed to decay exponentially with $(1 - M_c \cos\theta)^2$ (where M_c is the Mach number based on the phase velocity U_c of the convected wave), in agreement with the directivity of the models of Crow (1972) and Ffowcs Williams

& Kempton (1978). However, the excitation frequency corresponds to a Strouhal number, based on the jet diameter, of $St = 5.8$, which is much higher than the Strouhal numbers of the most energetic part of the sound field radiated by free turbulent jets. It is therefore difficult to affirm that Laufer & Yen's experiment corresponds to what occurs in unforced jet flows; the mechanism they studied is most likely to be restricted to low-Mach-number jets with laminar boundary layers at the nozzle exit, as discussed by Bridges & Hussain (1987).

On the other hand, Cavalieri *et al.* (2011*a*) have shown, with numerical data from a large-eddy simulation (LES) of a Mach 0.9 jet, that a simplified wavepacket *Ansatz*, fitted with velocity data from the LES, can reproduce the radiated sound for the axisymmetric mode of the simulation to within 1.5 dB at low polar angles. Furthermore, the axisymmetric mode was found to be highly directive, dominating sound radiation at low polar angles, as found experimentally by Fuchs & Michel (1978) and Juvé *et al.* (1979). These results suggest that the signature of a wavepacket source structure may be observable in high-Reynolds-number jets if the axisymmetric radiation is isolated from the other azimuthal modes present in the acoustic field.

The objective of the present work is to investigate, experimentally, if such superdirective wavepacket signatures are present in the acoustic field of *unforced* subsonic jets. We decompose the acoustic field measured by a microphone ring array into azimuthal Fourier modes. We then examine the directivity and spectra of each azimuthal mode; polar spacings of $\Delta\theta = 5^\circ$ are used at low emission angles, in order to obtain good angular resolution of the directivity of the different azimuthal modes, and to detect the expected high variations in acoustic intensity. We focus particularly on the axisymmetric mode, in an effort to characterize its structure and ascertain if it is consistent with existing wavepacket models.

In our evaluation of the experimental data we consider a model problem wherein the free-space wave equation is driven by a simplified line source; the form of the source is consistent with Lighthill's acoustic analogy. The model problem considered is not, of course, intended to correspond to the real flow, or to contain all of the physics of jet noise production; its purpose is to allow us to test hypotheses. On one hand we want to check for consistency between experimentally observed features of the sound field and hypothesized, acoustically important, features of the flow. On the other hand, we wish to rule out source features that are not consistent with the sound field: for example, a superdirective sound field at low Mach number cannot be produced by an acoustically compact source; an extended axial source region, with significant interference effects, is required to generate such an acoustic field (Crighton & Huerre 1990), and one of the conclusions of the analysis is that the sound radiated to low polar angles is indeed dominated by such a source.

The paper is organized as follows. In § 2 we describe the experimental setup. In § 3 there is a brief review of pertinent results concerning wavepacket sound radiation. This is followed by a presentation and general discussion of the experimental results in § 4. We first focus on the results for the Mach 0.6 jet and show that the axisymmetric mode dominates the peak-frequency acoustic field at low polar angles, and the sound pressure level (SPL) for $St = 0.2$ is shown to be in agreement with the superdirectivity predicted by non-compact wavepacket models. The same characteristics are observed for the lower-Mach-number jets ($M = 0.4$, $M = 0.5$). Next, the axial extent of the source is estimated using the wavepacket model of Crow (1972). In § 4.3 we explore the scaling of the different azimuthal modes as a function of Strouhal and Helmholtz numbers to evaluate non-compactness effects on the spectral shape of the individual modes. We consider in § 4.4 the

velocity dependence of the different azimuthal modes; the analysis provides a second estimate of the source axial extent which is consistent with the one made using the directivity (provided compressibility effects are correctly accounted for). Extrapolation of the present results to higher subsonic Mach numbers suggests that the dominance of the axisymmetric mode will be further enhanced as the Mach number is increased.

While the main focus of the present work is the axisymmetric mode, results for higher-order modes are also shown to be compatible with wavepacket radiation. A theoretical framework is developed in appendix B, and in § 5 we present comparisons of a model of sound radiation by helical wavepackets with the present experimental results.

2. Experimental setup

The experiments were performed in the 'Bruit et Vent' anechoic facility at the Centre d'Etudes Aérodynamiques et Thermiques (CEAT), Institut Pprime, Poitiers, France. A photo of the setup is shown in figure 3 below. Acoustic measurements were made for unheated jets, with acoustic Mach numbers ($M = U/c$, where U is the jet exit velocity and c the ambient sound speed) in the range $0.35 \leqslant M \leqslant 0.6$ with an increment of 0.05. The nozzle diameter, D, was 0.05 m. With these conditions, the Reynolds number, $\rho UD/\mu$, varies from 3.7×10^5 to 5.7×10^5, where ρ and μ are, respectively, the density and the viscosity at the nozzle exit. All but the lowest velocity lead to a Reynolds number above 4×10^5, which was seen by Viswanathan (2004) as a critical number above which sound radiation attains asymptotic spectral shapes.

The velocity field is considered in cylindrical coordinates (x, r, ϕ), where x is aligned with the jet axis, r is the radius and ϕ the azimuthal angle; spherical coordinates (R, θ, Φ) are used for the acoustic field, where R is the radius, θ is the polar angle measured from the downstream jet axis and Φ is the azimuthal angle. For both systems, the origin is at the nozzle exit. The three velocity components are denoted u_x, u_r and u_ϕ.

A convergent section was located upstream of the jet exit, with an area contraction of 31. This was followed by a straight circular section of length 150 mm; a boundary layer trip was used to force transition 135 mm upstream ($2.7D$) of the nozzle exit. Extensive hot-wire velocity measurements were made throughout the jet, including the nozzle exit plane. An *in situ* calibration of the hot wire was performed using Pitot tube measurements as reference values (Tutkun *et al.* 2009). The mean axial velocity fields are shown in figure 1 for Mach numbers of 0.4, 0.5 and 0.6. Aside from a slight lengthening of the potential core as the Mach number is increased, there are only small differences between the normalized mean velocity profiles for these jets.

Radial profiles of the velocity field in the nozzle exit plane were obtained with high spatial resolution both upstream and downstream of the exit plane in order to discern the character of the boundary layer. The results, shown in figure 2, indicate that the boundary layers (Bridges & Hussain 1987) are turbulent. The boundary layer and momentum thicknesses at the nozzle exit are shown in table 1. For these estimates, the Crocco–Busemann relation for unitary Prandtl number was used to determine the density across the boundary layer.

Six microphones were deployed on an azimuthal ring in the acoustic field with a fixed angle θ to the downstream jet axis. The setup is shown in figure 3. The ring has

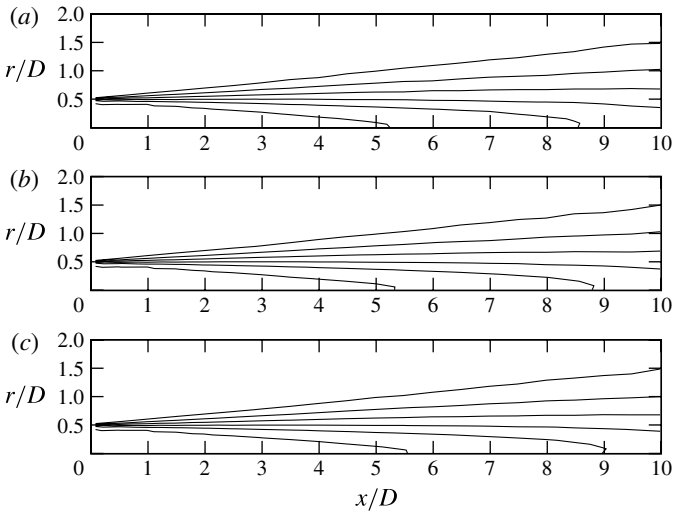

FIGURE 1. Mean axial velocity $\bar{u}_x$ fields for: (*a*) $M = 0.4$; (*b*) $M = 0.5$; and (*c*) $M = 0.6$. Contours are equally spaced from $0.1U$ to $0.99U$.

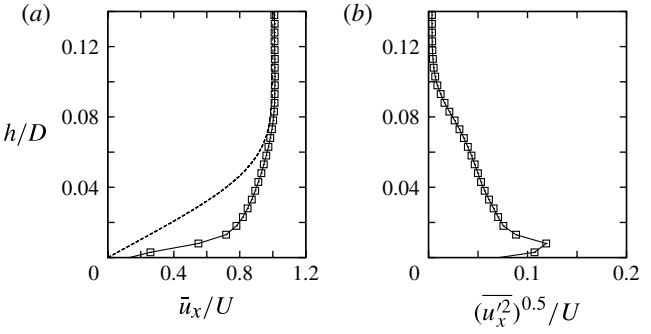

FIGURE 2. Boundary layer profiles at the nozzle exit for the Mach 0.5 jet: (*a*) mean velocity and (*b*) r.m.s. value. Dashed line in (*a*) is the Blasius profile.

M	δ (mm)	δ/D	δ_2 (mm)	δ_2/D
0.4	4.5	9.0×10^{-2}	0.477	9.5×10^{-3}
0.5	4.25	8.5×10^{-2}	0.401	8.0×10^{-3}
0.6	4.25	8.5×10^{-2}	0.396	7.9×10^{-3}

TABLE 1. Boundary layer thickness δ and momentum thickness δ_2 at the nozzle exit.

a diameter of $35D$. The entire array was displaced incrementally along the jet axis in order to characterize the sound field as a function of θ. On account of the resulting differences in the distance, R, between the nozzle exit and the microphones, a $1/R$ scaling is applied to the acoustic pressure in order to rescale the measurements to a fixed distance of $R = 35D$. The circumferential homogeneity of the acoustic field was

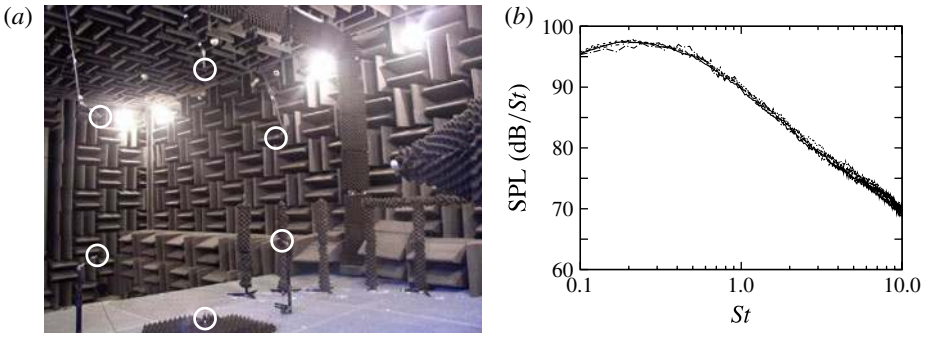

FIGURE 3. (Colour online) (*a*) Experimental setup (microphones are highlighted with white circles); (*b*) spectra of the six microphones at $\theta = 30^\circ$ and $M = 0.6$.

verified by comparing spectra of the individual microphones, shown in figure 3(*b*). The pressure from the six microphones was used to decompose the far acoustic field into azimuthal Fourier modes. The procedure is described in appendix A, where we also use the coherence between neighbouring microphones to assess the accuracy of the Fourier series. This evaluation shows that the procedure is appropriate up to Strouhal number of unity for the present microphone ring, which is the range of frequencies we focus on in the present work.

3. Sound radiation by an axisymmetric wavepacket

In this section we recall the results of Crow (1972) (see also Crighton 1975, § 10) for a simple wavepacket source. The results of this model are used for analysis of the experimental results presented in the following sections. The model is based on the acoustic analogy of Lighthill (1952). The continuity and Navier–Stokes equations are combined and rewritten as an inhomogeneous free-space wave equation with nonlinear source terms (Lighthill's stress tensor T_{ij}) on the right-hand side that depend on turbulent fluctuations:

$$\frac{\partial^2 \rho}{\partial t^2} - c^2 \nabla^2 \rho = \frac{\partial^2 T_{ij}}{\partial x_i \partial x_j} \tag{3.1}$$

with

$$T_{ij} = \rho u_i u_j + (p - c^2 \rho)\delta_{ij}. \tag{3.2}$$

In the spirit of the Lighthill's theory, the problem considered is an analogue of a compressible, turbulent flow. The source terms on the right-hand side of (3.1) are considered as given, and the radiated sound can be calculated, for a free jet, using the free-field Green's function.

In Crow's model, the wave equation is driven by a simplified line source S_{xx}, constructed using the axisymmetric part of the T_{xx} term alone (i.e. a distribution of axially aligned, longitudinal quadrupoles), as

$$S_{xx}(x, m = 0, \omega) = \int T_{xx}(x, r, m = 0, \omega) r \, \mathrm{d}r \tag{3.3}$$

where m is the azimuthal Fourier mode, and ω the frequency, so that the far-field pressure is given, as shown in appendix B, as

$$p(R,\theta,m=0,\omega) = -\frac{k_a^2\cos^2\theta \mathrm{e}^{-\mathrm{i}k_aR}}{2R}\int_{-\infty}^{\infty} S_{xx}(x,m=0,\omega)\mathrm{e}^{-\mathrm{i}k_ax\cos\theta}\,\mathrm{d}x, \tag{3.4}$$

where k_a is the acoustic wavenumber ω/c.

This line source model comprises a convected wave of frequency ω and wavenumber k, modulated by a Gaussian with characteristic length L,

$$S_{xx}(x,m=0,\omega) = \rho_0 U\hat{u}_x\frac{D^2}{4}\mathrm{e}^{-\mathrm{i}kx}\mathrm{e}^{-x^2/L^2}, \tag{3.5}$$

where ρ_0 is the density of the undisturbed fluid and $\hat{u}_x$ the streamwise velocity fluctuation amplitude, which is obtained by the radial integration in (3.3) of a radially constant T_{xx}, given as

$$T_{xx}(x,r,m=0,\omega) = 2\rho_0 U\hat{u}_x\mathrm{e}^{-\mathrm{i}kx}\mathrm{e}^{-x^2/L^2} \tag{3.6}$$

between 0 and $D/2$. An envelope function given by a Gaussian, as in (3.6), is supported by the near-field measurements of forced jets by Laufer & Yen (1983), and of unforced, heated jets with Mach numbers ranging from 0.9 to 1.58 (Reba, Narayanan & Colonius 2010). Gaussian envelopes were also seen to match envelopes taken from the velocity field of large-eddy simulations of cold $M = 0.9$ jets (Cavalieri *et al.* 2011*b*). Finally, the experimental near-field pressure results presented by Gudmundsson & Colonius (2011), including an unheated jet at $M = 0.5$ and $Re = 7\times10^5$, suggest that a Gaussian envelope may be appropriate to model wavepackets in jets with the operating conditions of the present work.

The line-source approximation in (3.6) can be justified in Lighthill's analogy for the axisymmetric part of the source if we consider radial compactness, i.e. the jet diameter is much smaller than the acoustic wavelength, as shown in appendix B. This is the case for low values of the Strouhal and Mach numbers.

Furthermore, in a linear problem, such as Lighthill's, a given azimuthal component of the source generates the same azimuthal mode in the sound field. This assumption has been used, for instance, by Michalke (1970, 1972) or Mankbadi & Liu (1984), and is also shown in the derivation of appendix B. The line-source model in (3.6) is therefore solely related to the axisymmetric radiation. A similar model for helical wavepackets is presented in § 5.

Evaluation of the far-field pressure in the time domain leads to

$$p(R,\theta,m=0,t) = -\frac{\rho_0 U\tilde{u}M_c^2\,(kD)^2\,L\sqrt{\pi}\cos^2\theta}{8R} \times \exp[-L^2k^2\,(1-M_c\cos\theta)^2\,/4]\exp[\mathrm{i}\omega\,(t-(R/c))], \tag{3.7}$$

where M_c is the Mach number based on the phase velocity U_c of the convected wave. The acoustic intensity in the far acoustic field can be calculated as $p^2/(\rho_0 c)$.

The models of Ffowcs Williams & Kempton (1978) and Cavalieri *et al.* (2011*b*), which include jitter in this source shape, also present the same exponential function $\exp(-L^2k^2\,(1-M_c\cos\theta)^2\,/4)$ for the pressure. This exponential polar variation is referred to as *superdirectivity* (Crighton & Huerre 1990).

We note that superdirectivity results if the characteristic length, L, of the Gaussian is large compared to the convected wavelength, i.e. $kL = 2\pi L/\lambda_c \gg 1$.

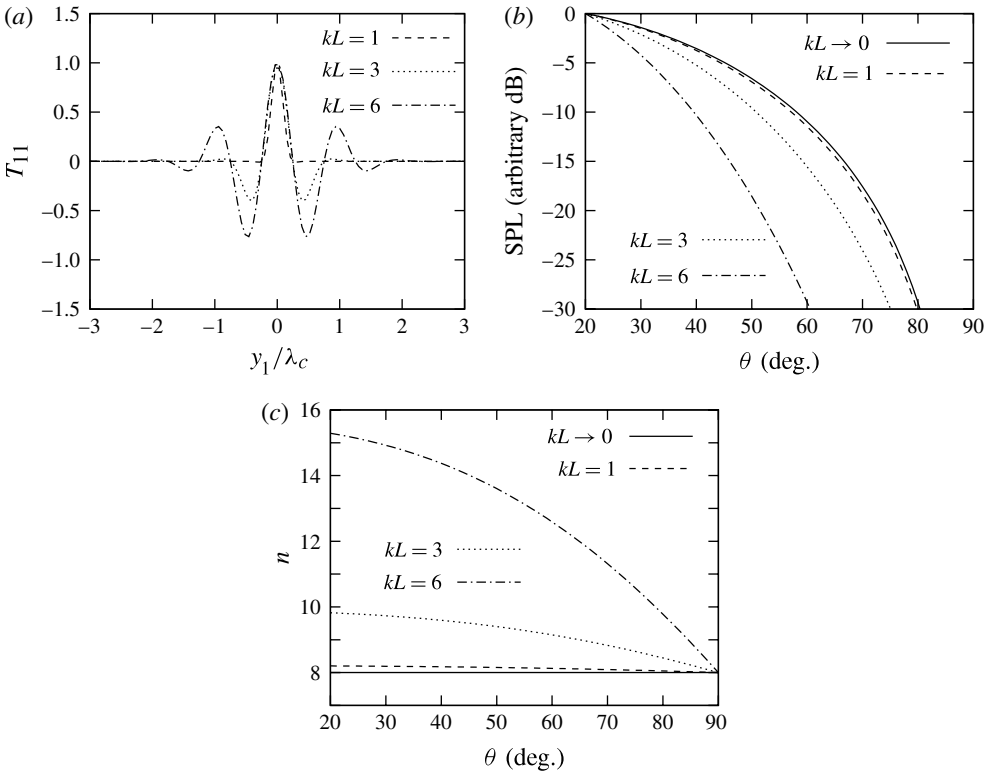

FIGURE 4. (*a*) Wavepacket shapes, (*b*) corresponding directivities for $M_c = 0.36$ with values at $\theta = 20°$ fixed at 0 dB, and (*c*) velocity exponents, taken with a derivative around $M_c = 0.3$.

The superdirectivity can thus be seen to result from axial interference in an axially extended source comprising more than one oscillation wavelength. For subsonic convection velocities, the interference between regions of positive and negative source strength results in the sound field being beamed towards low angles, an almost complete cut-off occurring at high polar angles. This is illustrated in figure 4, where source shapes and corresponding directivities are plotted for different values of kL, considering $M_c = 0.36$. For the compact limit, $kL \to 0$, the directivity of the source is given by $\cos^4\theta$ for the acoustic intensity. For small values of the characteristic length, L, the dependence of the directivity on L is weak. However, as the axial interference becomes significant, the directivity changes considerably, becoming increasingly concentrated at low axial angles, as can be seen in figure 4(*b*) for $kL = 6$. In this case, the directivity shape is dominated by the exponential term in (3.7), and is close to a straight line when plotted as a function of $(1 - M_c \cos\theta)^2$. For this source extent, as shown in figure 4(*a*), there is interference between three neighbouring wavefronts in the source, leading to the observed superdirectivity.

It is clear that the theoretical directivity shape is not purely exponential, and that the $\cos^2\theta$ term in (3.7) causes deviations from a straight line when the acoustic intensity is plotted in dB as a function of $(1 - M_c \cos\theta)^2$. However, for the non-compact wavepackets educed in the following sections, which have typical extensions leading to $kL \approx 6$, the deviations of such a plot from a fitted straight line are lower than 0.5 dB, and cannot be clearly discerned in the present set of experimental results.

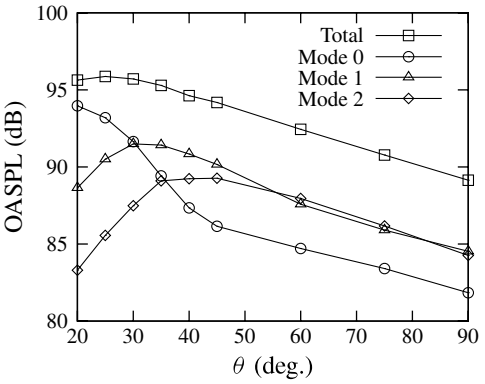

FIGURE 5. Directivity for the $M = 0.6$ jet.

Based on this we have chosen to evaluate superdirectivity in our measurements by a comparison of SPL as a function of $(1 - M_c \cos\theta)^2$ with straight lines. The $\cos^2\theta$ factor in acoustic pressure is nonetheless accounted for in all estimations of kL made in § 4.

A further effect of non-compactness can be seen in the velocity dependence of sound radiation. A compact source will lead to a U^8 velocity dependence of the acoustic intensity. But as non-compact effects become significant, the velocity dependence changes, and may be other than a power law; indeed, the expression in (3.7) is not a power law in the velocity. Figure 4(*c*) shows the velocity exponent, n, of the acoustic intensity for $M = 0.5$, evaluated using (3.7). For this calculation we assume constant Strouhal number and source extent, L/D. We note that a compact wavepacket, with, for example $kL = 1$, has a velocity exponent close to 8 for all angles; increases in L lead to higher velocity exponents, especially for lower axial angles.

4. Experimental results and analysis

4.1. *Mach* 0.6 *jet*

Figure 5 shows the directivity of the Mach 0.6 jet for the measured angles, as well as the contributions of the different azimuthal modes. The axisymmetric mode presents a marked directivity towards the low axial angles. Indeed, there is a 7.8 dB increase in the overall sound pressure level (OASPL) between 45° and 20°. The other azimuthal modes increase more gradually over $45° \leqslant \theta \leqslant 90°$, with a slope close that of the axisymmetric mode in the same angular sector. For lower angles, modes 1 and 2 decay with decreasing angle. Similar directivities for the azimuthal modes 0, 1 and 2 have been observed in a large-eddy simulation of a Mach 0.9 jet (Cavalieri *et al.* 2011*a*).

Spectra for angles 20°, 30° and 40° are shown in figure 6. The increase of mode 0 is mostly concentrated in the lower frequencies. For Strouhal numbers greater than 1 there is still a dominance in the total spectra of modes 1 and 2.

To evaluate the directivity of the spectral peak, the SPL for $St = 0.2$ is shown in figure 7. We see that for this frequency there is an even higher directivity of mode 0, with an increase of 15.4 dB between 45° and 20°, i.e. a factor of 34 in the acoustic intensity.

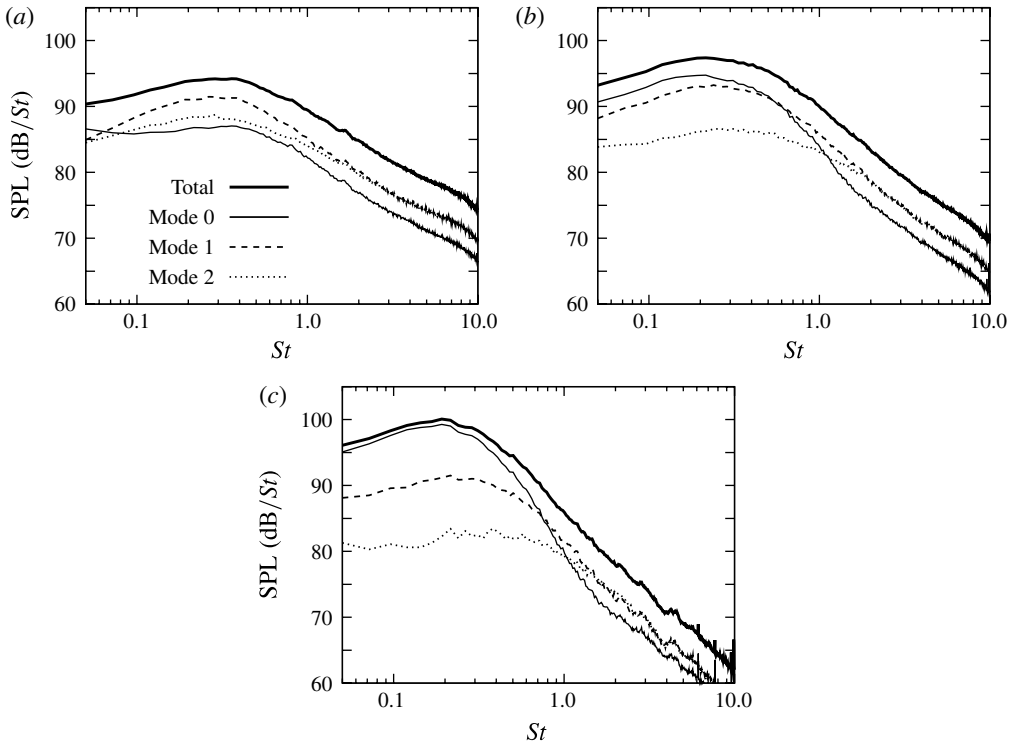

FIGURE 6. Spectra of individual modes for (*a*) $\theta = 40°$, (*b*) $\theta = 30°$ and (*c*) $\theta = 20°$.

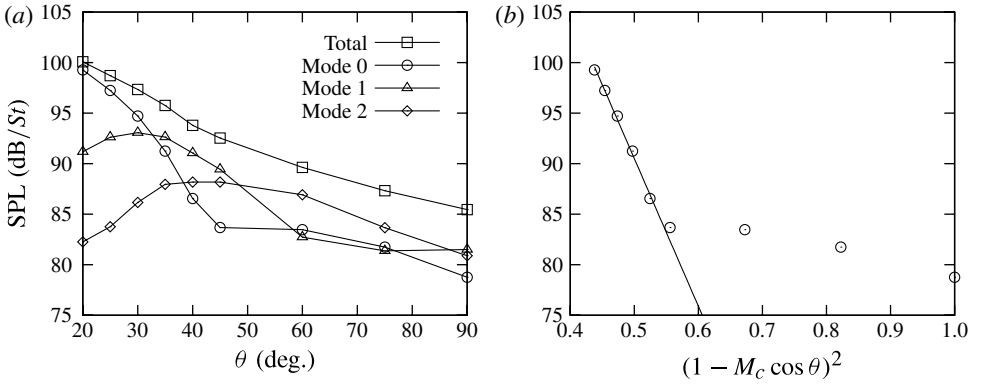

FIGURE 7. SPL for $St = 0.2$ for the Mach 0.6 jet as a function of (*a*) θ and (*b*) $(1 - M_c \cos\theta)^2$.

As presented in § 3, models representing the wavepacket form of axisymmetric coherent structures in jets predict an exponential change of sound intensity with $(1 - M_c \cos\theta)^2$. Figure 7(*b*) presents the SPL at $St = 0.2$ as a function of this parameter, considering M_c to be equal to $0.6M$; changes in M_c from 0.5 to 0.7 were seen to have little impact on the directivity shape. The constant slope in the sector $20° \leqslant \theta \leqslant 45°$ indicates that there is indeed an exponential change. Furthermore,

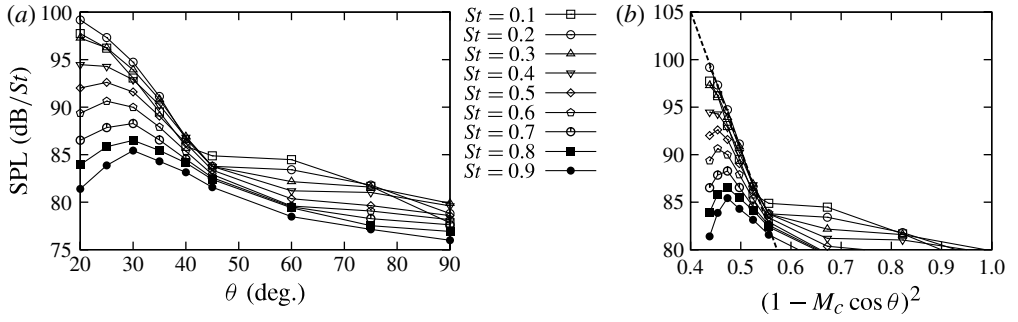

FIGURE 8. Directivity for the axisymmetric mode as a function of Strouhal number and of (*a*) θ and (*b*) $(1 - M_c \cos\theta)^2$.

since these models are based on a line-source distribution, the radiated sound field is axisymmetric. The comparison with the experimental mode 0 is thus justified.

The directivity shape of azimuthal modes 1 and 2 in figure 7 is shown in § 5 to be compatible with a source constituted of helical wavepackets, which do not produce superdirective radiation. Further discussion of the higher azimuthal modes is postponed to § 5, where a model for the sound radiation by helical wavepackets is developed.

The superdirectivity observed for the axisymmetric mode is present for a range of frequencies near the peak as can be seen in figure 8. We note that for $0.1 \leqslant St \leqslant 0.3$ the directivity changes very little, and a linear fit made for $St = 0.2$ closely matches the directivity for both $St = 0.1$ and $St = 0.3$. For higher frequencies, we note that as the angle is increased, the SPL tends to the same exponential decay observed for the peak frequency. As the frequency is increased, this decay is progressively less significant: whereas a decay of 15.4 dB between 20° and 45° is observed for $St = 0.2$, for $St = 0.4$ we have a decay of 10.7 dB, and for $St = 0.6$ we have 7.7 dB (now between 25° and 45°, for the maximum level is obtained for $\theta = 25°$). Although the decay at higher St differs from that at $St = 0.2$, the high-frequency directivity remains exponential, as seen in figure 9 for $St = 0.4$, 0.6 and 0.8, but with progressively lower slopes. The deviations from the straight lines for low angles (20° and 25°) that are measured for higher frequencies may be due to propagation effects; this is discussed in more detail in the following section.

The results of figure 8 and the mode-0 spectra shown in figure 6 suggest that the results for $St = 0.2$ are representative of a range of frequencies around the spectral peak.

4.2. *Lower Mach numbers*

The trends observed in the $M = 0.6$ jet were also found for the lower-Mach-number flows. Figures 10 and 11 show spectra for $M = 0.4$ and $M = 0.5$, respectively. The results are similar to the $M = 0.6$ jet. However, we note that as the Mach number is reduced, the dominance of the axisymmetric mode at, say, $\theta = 20°$ or $\theta = 30°$ is decreased. This effect in the OASPL is shown in figure 12, and for the SPL at $St = 0.2$ in figure 13. For convenience, we replot, in both figures, the results for the $M = 0.6$ jet.

For $M = 0.4$ to $M = 0.6$, the SPL at $St = 0.2$ is shown as a function of $(1 - M_c \cos\theta)^2$ in figure 14. We note once more the same trends for all three

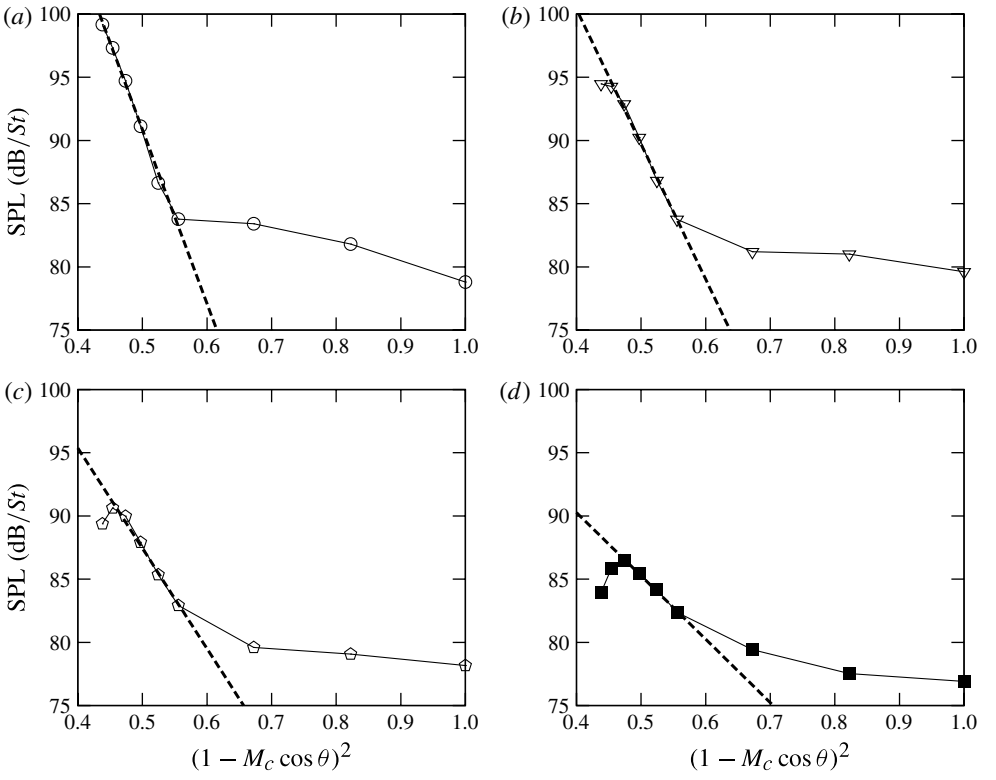

FIGURE 9. Directivity for the axisymmetric mode as a function of $(1 - M_c \cos\theta)^2$ for (*a*) $St = 0.2$, (*b*) $St = 0.4$, (*c*) $St = 0.6$ and (*d*) $St = 0.8$.

Mach numbers, with an exponential decay of the acoustic intensity as a function of $(1 - M_c \cos\theta)^2$, indicating again the superdirectivity of the axisymmetric mode.

The behaviour observed at other frequencies is shown in figure 15 for $M = 0.4$ and $M = 0.5$. The $M = 0.6$ results are repeated for convenience. We note that for the three cases the directivity shapes for $St = 0.1$ and 0.3 closely follow the straight line fitted for $St = 0.2$, showing that superdirectivity is present over a range of frequencies. Moreover, as the Mach number decreases, a broader range of frequencies have directivities close to that of the $St = 0.2$ component: the change of slope observed with increasing St, shown in figure 9 for $M = 0.6$, is less significant at lower Mach numbers.

Another feature of the directivity shapes in figure 15 is that for high frequencies there is a departure from the superdirective behaviour, a reduction of SPL occurring at the lower angles. This is especially marked for $M = 0.6$ at Strouhal numbers of 0.5 and above. For lower Mach numbers the effect is significantly reduced. A possible explanation can be given in terms of propagation effects such as refraction by the mean shear, which tends to decrease the sound at low polar angles, especially at higher Mach number. This is not accounted for by the simplified model of (3.6) and (3.7), which is based on Lighthill's analogy. This point merits further study, but is outside the scope of the present work.

Since the directivity for $St = 0.2$ is exponential between $\theta = 20°$ and $\theta = 45°$, we can use the measured exponential decay rate to estimate the wavepacket axial

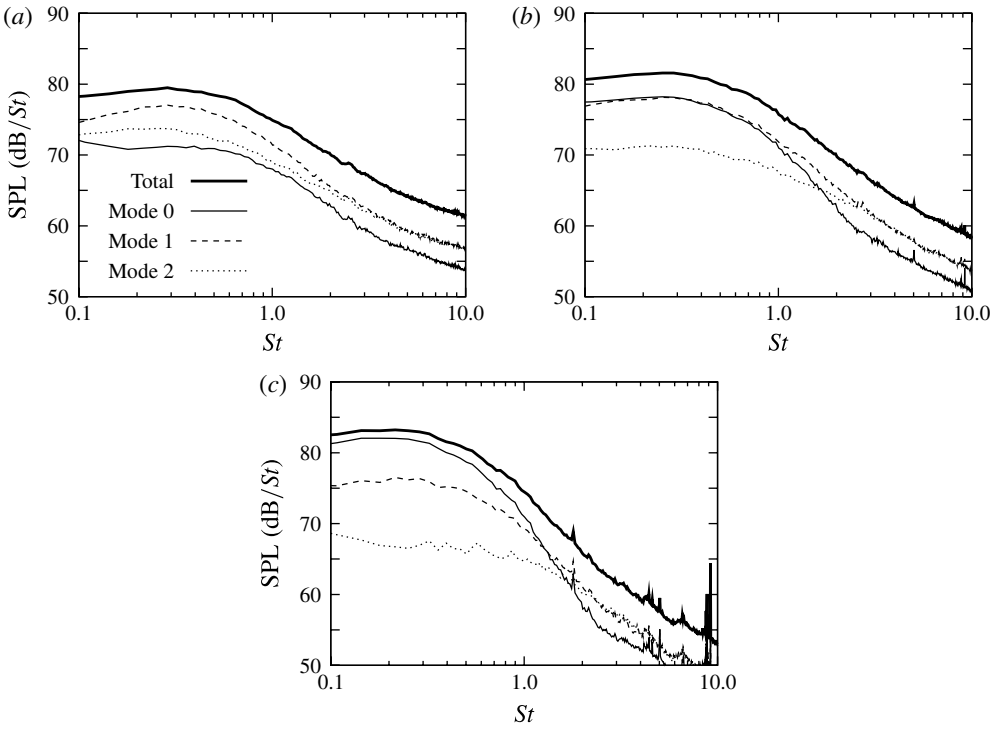

FIGURE 10. Spectra of individual modes for $M = 0.4$ and (*a*) $\theta = 40°$, (*b*) $\theta = 30°$ and (*c*) $\theta = 20°$.

M	SPL($\theta = 20°$) − SPL($\theta = 45°$) (dB)	kL	L/D
0.4	13.2	6.50	3.10
0.5	14.1	6.34	3.03
0.6	15.4	6.40	3.06

TABLE 2. Estimation of source extent using the axisymmetric mode at $St = 0.2$.

extent, L/D, via the wavepacket *Ansatz* described in § 3 and an assumed value of $U_c/U = 0.6$. A best fit of the experimental data then results in the estimated values of L/D given in table 2.

The use of Crow's wavepacket model results in a consistent estimation of L/D for all three Mach numbers, with a value close to 3. In turn, this value of L/D indicates that the wavepacket extends over an axial region of 6–8 jet diameters, similar to the result shown in figure 4(*a*) for $kL = 6$ (setting $U_c/U = 0.6$ and $St = 0.2$, $\lambda_c = 3D$). This modulation is such that three oscillations are present in the source; i.e. there is significant axial interference, as discussed in § 3, leading to the observed superdirectivity in the radiated sound field.

The above estimate of the axial source extent is in agreement with results reported by Hussain & Zaman (1981), who educed, using phase-averaged measurements in a jet excited at $St = 0.3$, a flow pattern comprising a train of three coherent structures,

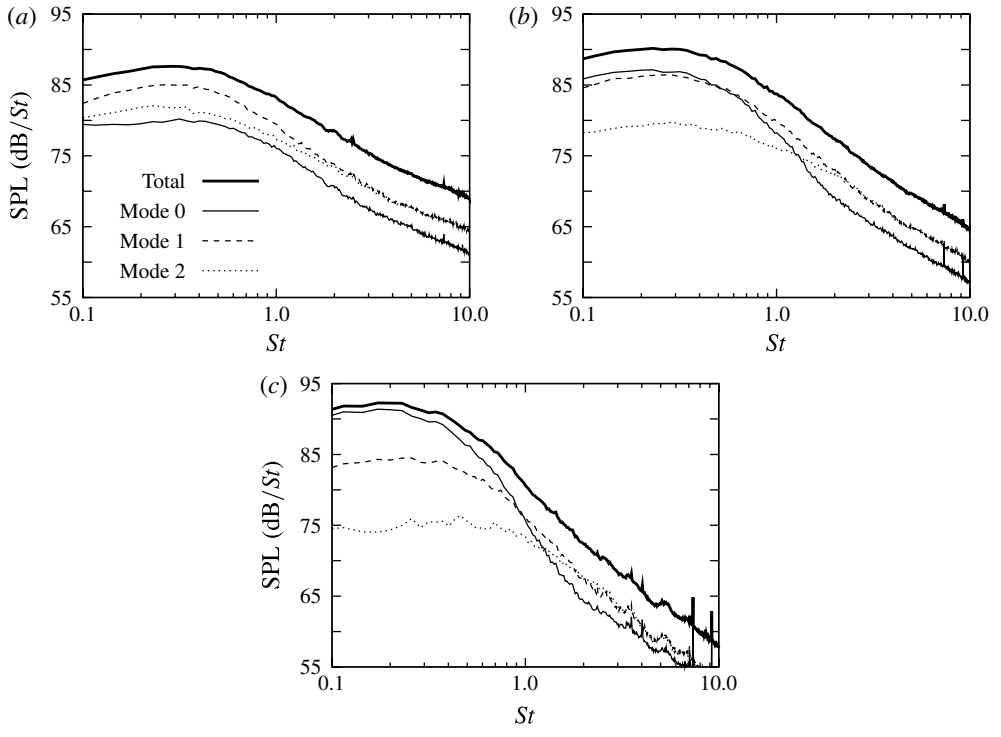

FIGURE 11. Spectra of individual modes for $M = 0.5$ and (*a*) $\theta = 40°$, (*b*) $\theta = 30°$ and (*c*) $\theta = 20°$.

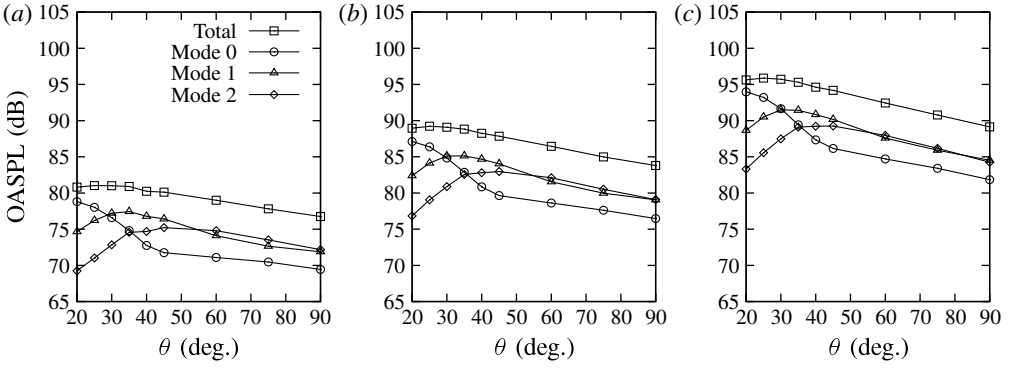

FIGURE 12. Directivity for (*a*) $M = 0.4$, (*b*) $M = 0.5$ and (*c*) $M = 0.6$.

characterized by regions of closed vorticity contours, and spanning a region of up to 7 jet diameters from the nozzle exit. This also agrees with the experimental observations of Tinney & Jordan (2008), who studied the near pressure field of unforced coaxial jets, and found a subsonically convected wave extending up to 8 secondary jet diameters downstream of the nozzle exit. In their study, the first two proper orthogonal decomposition (POD) modes of the near-field pressure had the

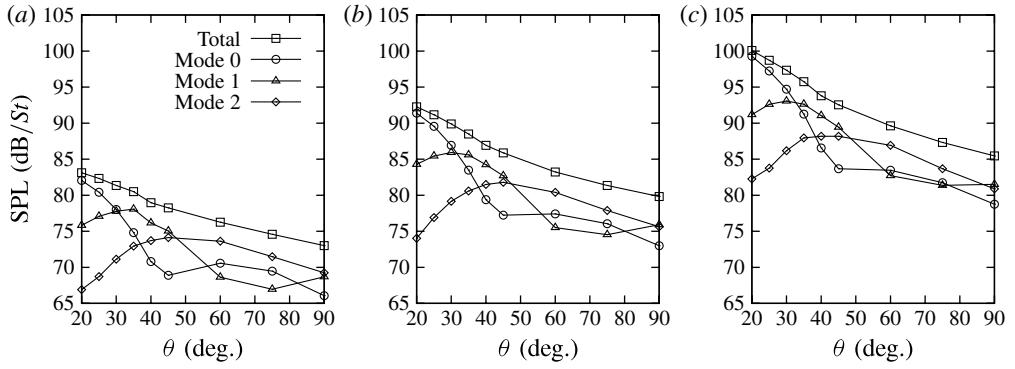

FIGURE 13. SPL for $St = 0.2$: (*a*) $M = 0.4$, (*b*) $M = 0.5$ and (*c*) $M = 0.6$.

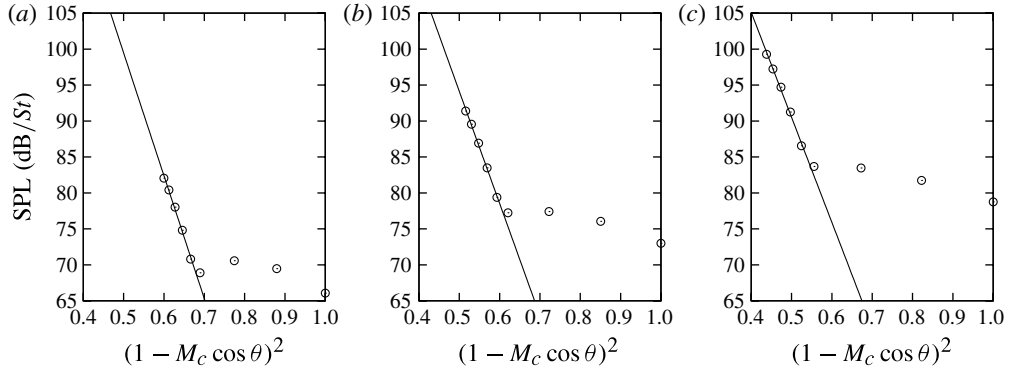

FIGURE 14. SPL of the axisymmetric mode for $St = 0.2$ and (*a*) $M = 0.4$, (*b*) $M = 0.5$ and (*c*) $M = 0.6$.

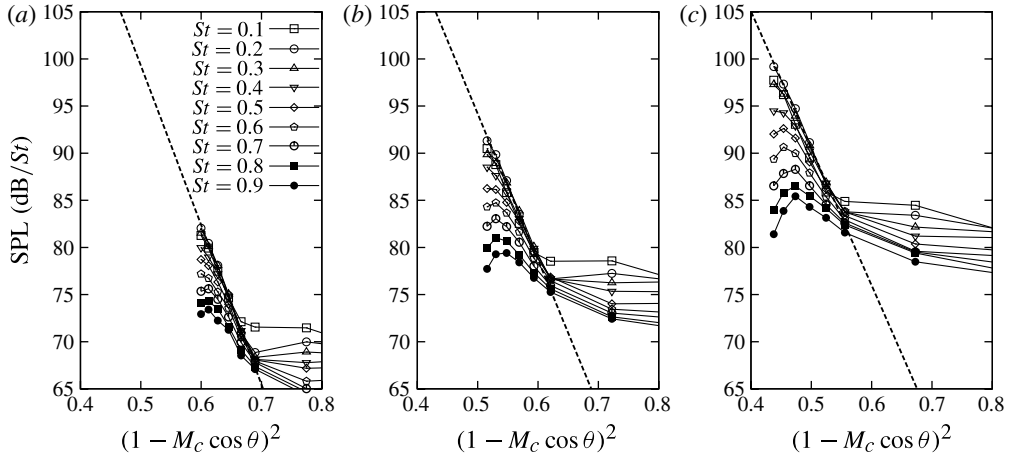

FIGURE 15. SPL of the axisymmetric mode as a function of $(1 - M_c \cos\theta)^2$ for (*a*) $M = 0.4$, (*b*) $M = 0.5$ and (*c*) $M = 0.6$.

M	$\mathrm{SPL}(\theta = 20°) - \mathrm{SPL}(\theta = 45°)$ (dB)	kL	L/D
0.4	11.8	5.94	1.42
0.5	11.8	5.48	1.31
0.6	10.7	4.75	1.13

TABLE 3. Estimation of source extent using the axisymmetric mode at $St = 0.4$.

M	$\mathrm{SPL}(\theta = 25°) - \mathrm{SPL}(\theta = 45°)$ (dB)	kL	L/D
0.4	8.8	5.18	0.82
0.5	8.3	4.50	0.72
0.6	7.7	3.92	0.62

TABLE 4. Estimation of source extent using the axisymmetric mode at $St = 0.6$.

M	$\mathrm{SPL}(\theta = 30°) - \mathrm{SPL}(\theta = 45°)$ (dB)	kL	L/D
0.4	6.1	4.38	0.46
0.5	5.1	3.16	0.42
0.6	4.1	1.81	0.29

TABLE 5. Estimation of source extent using the axisymmetric mode at $St = 0.8$.

shape of a sine and a cosine modulated by an envelope function comprising three oscillation cycles.

The same estimation was performed using the directivities observed at $St = 0.4$, 0.6 and 0.8, and the results are shown in tables 3–5, respectively. For the Mach 0.4 jet the estimated source extent for $St = 0.4$ is roughly half that estimated for $St = 0.2$. Since the wavelength of the convected wave is also halved as the Strouhal number is increased, this means that in this case the source also presents three spatial oscillations. As the Mach number is increased the estimated values of L/D are reduced; however, this does not mean that the source becomes compact, since we are still far from the $kL \to 0$ limit, as seen in § 3. Estimation of the source extent for $St = 0.6$ shows similar trends to those observed at $St = 0.4$. The estimated values of L/D become lower as the Mach number is increased, but the wave-like behaviour of the source is preserved.

For $St = 0.8$ the source extent is substantially reduced at higher Mach number, and for $M = 0.6$ we have a value of kL of 1.8, approaching the compact limit. However, the apparent 'cone of silence' observed in this case (see figure 15) suggests that the estimation of the source extent may be biased here by flow-acoustic effects.

4.3. *Spectral shape for the different azimuthal modes*

We now examine the scaling of the spectra with Mach number. Figures 16 and 17 show, respectively for the axisymmetric and first azimuthal mode, the spectra normalized by their maximum values, and plotted versus either Strouhal number, fD/U, or Helmholtz number, fD/c. The spectra of the axisymmetric component of the sound field collapse better when plotted as a function of Helmholtz number, whereas azimuthal mode 1 collapses better when plotted as a function of Strouhal number.

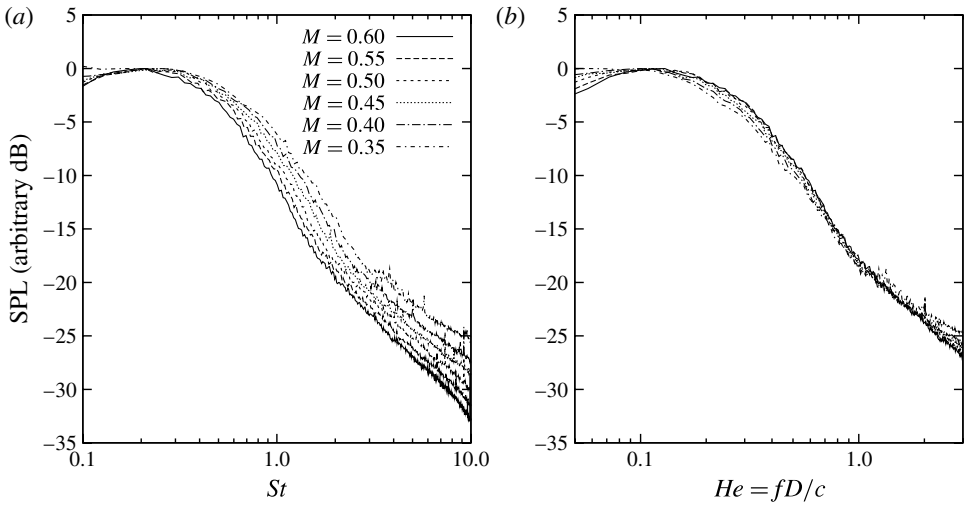

FIGURE 16. Spectral shapes for azimuthal mode 0 and $\theta = 30°$ as a function of (*a*) Strouhal number and (*b*) Helmholtz number.

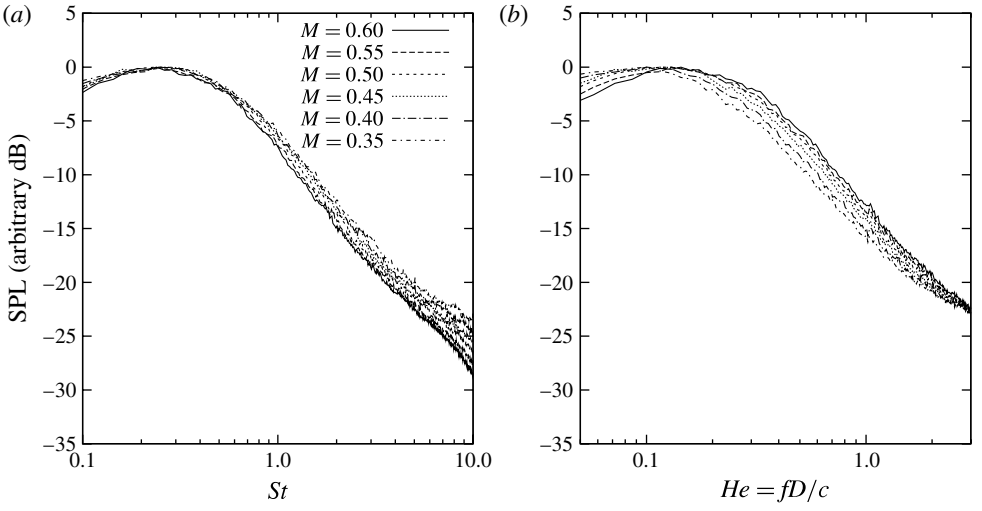

FIGURE 17. Spectral shapes for azimuthal mode 1 and $\theta = 30°$ as a function of (*a*) Strouhal number and (*b*) Helmholtz number.

The Helmholtz number is related to the source compactness, as $He = D/\lambda$, where λ is the acoustic wavelength. If the source extent is comparable to the acoustic wavelength, the Helmholtz number will play a significant role, for it is a measure of the interference effects from the different parts of the source; discussion of the significance of the Helmholtz number for aeroacoustic applications can be found in the work of Fuchs & Armstrong (1978). The scaling of the axisymmetric mode with the Helmholtz number suggests again that the non-compactness of the source plays an important role in the radiation of sound to low axial angles. The scaling of low-

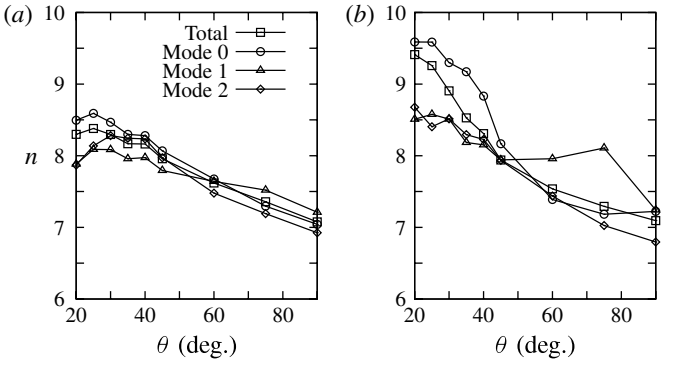

FIGURE 18. Velocity exponent n obtained by fits of (a) the OASPL and (b) SPL for $St = 0.2$.

angle spectra with Helmholtz number (without separation into azimuthal modes) has been observed previously by Lush (1971), Tanna (1977) and Viswanathan (2004). We show here that as the axisymmetric mode accounts for most of the radiation at these angles, the *He* scaling in the total spectrum is predominantly due to the axisymmetric component. On the other hand, the Strouhal number scaling found, for instance at 90° to the jet axis, can be related to the mode-1 scaling with St, seen in figure 17(a), as at higher angles the axisymmetric radiation is no longer dominant.

4.4. *Velocity dependence of the sound radiation for each azimuthal mode*

Close examination of figure 12 shows that the velocity dependence of the OASPL at each angle is not the same for the different azimuthal modes. Such variations are also observed in the SPL for $St = 0.2$, shown in figure 13. In order to evaluate this velocity dependence as a function of both θ and azimuthal mode, we performed fits of both OASPL and SPL for $St = 0.2$ as

$$\mathrm{OASPL(dB)}(m,\theta) = a(m,\theta) + 10n(m,\theta)\log_{10}(M), \tag{4.1}$$

$$\mathrm{SPL(dB/}St\mathrm{)}(m,\theta) = a(m,\theta) + 10n(m,\theta)\log_{10}(M), \tag{4.2}$$

respectively, to obtain velocity scalings of the sound radiation, as in previous work (Zaman & Yu 1985; Viswanathan 2006; Bogey *et al.* 2007). This was done for the total values of OASPL and SPL, and also for the individual contributions of azimuthal modes 0, 1 and 2. Results are shown in figure 18.

The velocity exponents for OASPL shown in figure 18(a) do not show clear trends among the different azimuthal modes for higher angles. However, we note that for low angles the mode-0 exponent is higher than both those of the other azimuthal modes and of the total spectrum. If we extrapolate these trends for higher Mach numbers, we can expect that for low angles the mode-0 dominance in OASPL will be even more pronounced.

Considering the velocity dependence of SPL for $St = 0.2$ alone, shown in figure 18(b), these effects are even more marked, the velocity exponent of the axisymmetric mode for low angles being considerably higher than that of the other modes. This, as shown in § 3, is another indication of non-compactness of the source.

Naive use of the values obtained for n for $St = 0.2$ to estimate the source length based on the wavepacket model of § 3 leads to a source extent of $L/D \approx 1.5$ (source extent of 3–4 jet diameters) which is roughly half that estimated in § 4.3 based on the directivity. However, the derivation of the velocity exponent with the Crow (1972)

wavepacket model assumes that the source extent and maximum amplitude do not change with increasing Mach number, and it also assumes a constant ratio between convection and jet speeds. Moreover, compressibility affects the development of the velocity fluctuations as a function of Mach number (see Lele 1994 and references therein for studies on compressible mixing layers). Linear stability theory also predicts lower growth rates as the Mach number is increased (see, for instance, reviews by Michalke (1984) and Morris (2010)).

Velocity spectra on the jet centreline are shown in figure 19(*a,b*) for $x = 2D$ and $x = 4D$. The centreline spectrum is chosen to highlight the axisymmetric mode of the velocity fluctuations. In stability theory the boundary conditions on the jet centreline are of zero transverse velocity and arbitrary finite streamwise velocity for $m = 0$, and zero streamwise velocity for all higher-order azimuthal modes (Batchelor & Gill 1962); therefore, we expect the centreline spectrum to be representative of the axisymmetric mode; indeed, such measurements have been used in the past for comparison with stability results (Crow & Champagne 1971; Michalke 1971; Crighton & Gaster 1976).

We see that for both axial positions the amplitude of the velocity fluctuations, when normalized by the jet velocity, decreases as the Mach number is increased. This can be attributed to the lower growth rate predicted by stability theory for higher Mach numbers, since the differences in the mean velocity profiles are slight (see figure 1) and could not cause such a significant effect. The reduction of the normalized amplitude for higher Mach numbers was also observed by Armstrong, Fuchs & Michalke (1977) and Suzuki & Colonius (2006) in experimental results for the near-field pressure. On the other hand, for the velocity spectra on the jet lipline, shown in figure 19(*c*), the results for the three Mach numbers collapse. The variation of the Mach number from 0.4 to 0.6 therefore has a significant effect on the evolution of the axisymmetric mode, but no detectable effect on the full jet turbulence.

This suggests that in order to appropriately account for the velocity dependence in the axisymmetric wavepacket model of § 3, one should account for the reduction of the normalized amplitude $\hat{u}_x/U$ as the Mach number is increased, leading to lower velocity exponents than the results of figure 4(*c*). To perform an estimation of the source extent that accounts for compressibility effects in the evaluation of n, we have plotted in figure 20 the power spectral density for the centreline velocity for $St = 0.2$. We note that the decrease in the power can be roughly approximated by the straight line in the figure with a slope of -1.8. Using this expression in the evaluation of the velocity exponent n of the sound radiation of Crow's wavepacket model we obtain the results shown in figure 20(*b*). The exponents for $kL = 6$ are close to the experimental values in the angular range $20^\circ \leqslant \theta \leqslant 45^\circ$ where superdirectivity was observed, consistent with the value of kL educed from the directivity in § 4.2.

Although the use of a velocity exponent n is useful to scale jet data at different Mach numbers and predict the increase of sound level as the jet velocity increases, it should be noted that non-compact sources, such as are described by the wavepacket model of (3.7), lead to a velocity dependence for the sound intensity that departs from a U^n form. As the Mach-number range of the present tests is not comprehensive, a conclusive answer is not at present available regarding the precise form of the velocity dependence for the different azimuthal modes. Deviations from a U^n law can be seen in the results of Lush (1971), which spanned Mach numbers from 0.3 to 1.

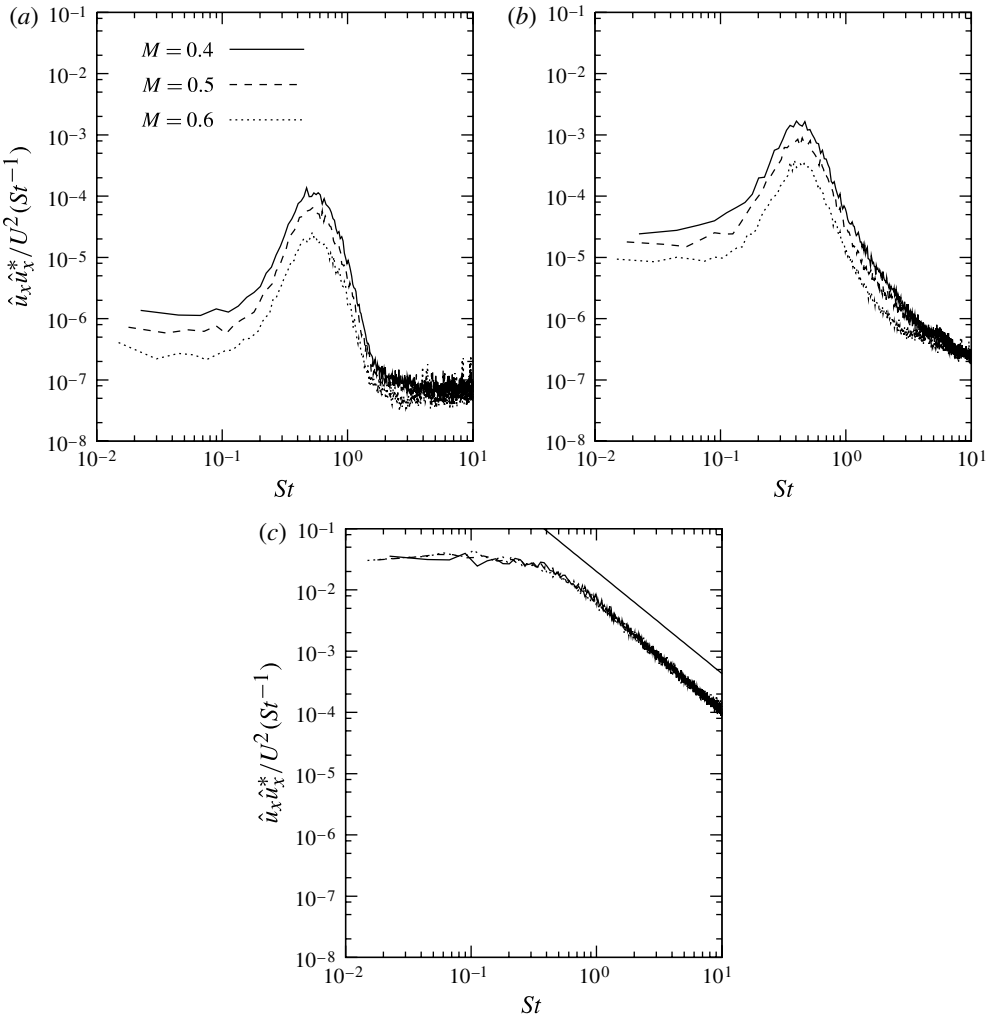

FIGURE 19. Velocity spectra on the jet centreline for (*a*) $x = 2D$ and (*b*) $x = 4D$, and (*c*) on the jet lipline for $x = 2D$. The straight line in (*c*) represents a $-5/3$ slope.

5. Sound radiation by helical wavepackets

The far-field sound radiation from a given azimuthal mode of the T_{xx} component of Lighthill's stress tensor, derived in appendix B, is

$$p(R, \theta, m, \omega) = -\frac{\mathrm{i}^m k_a^2 \cos^2\theta \mathrm{e}^{-\mathrm{i}k_a R}}{2R} \int \mathrm{e}^{\mathrm{i}k_{ax}\cos\theta}\,\mathrm{d}x \int T_{xx}(x, r, m, \omega) \times \mathrm{J}_m(k_a r \sin\theta) r\,\mathrm{d}r. \tag{5.1}$$

The line-source approximation, used in the analysis of the preceding section, and derived in appendix B for the axisymmetric mode, cannot be applied for the other azimuthal modes. The reason is the presence of $\sin\theta$ in the argument of the Bessel function in (5.1); even though equivalent line sources can be obtained after the radial

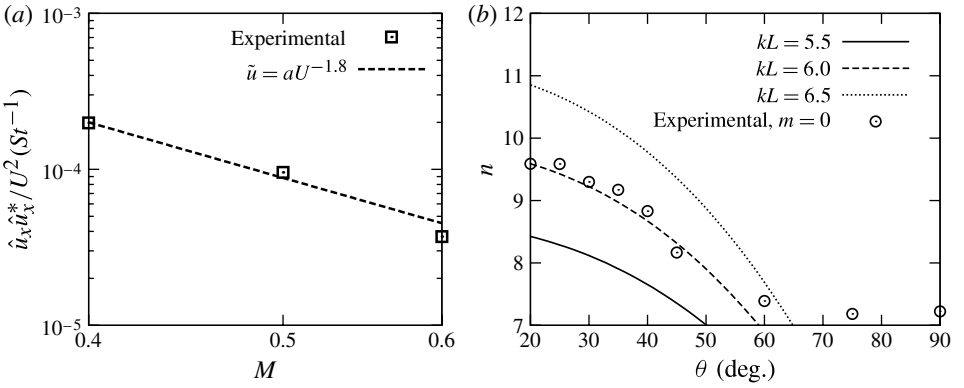

FIGURE 20. (*a*) Velocity dependence of the power spectral density of the centreline velocity at $x = 4D$ for $St = 0.2$, (*b*) velocity exponent of sound radiation by wavepackets assuming $\tilde{u} = aU^{-1.8}$.

integration, a different line distribution is obtained for each polar angle, and hence no single line source is valid for all θ.

Another difference when we evaluate the sound radiation for a helical mode is that the radial distribution of fluctuations plays a significant role, even for small frequencies and Mach numbers. The Bessel functions of first kind of order m are proportional to x^m for low x; thus, for the axisymmetric mode they can be approximated as constant, whereas for the other azimuthal modes their precise shape will influence the result of the radial integral in (5.1). Moreover, the assumption that the axial velocity fluctuations do not change radially, used in Crow's model, can only be used for the axisymmetric mode, since for helical modes the axial velocity fluctuation on the jet centreline is zero (Batchelor & Gill 1962).

In order to obtain the directivity of the sound radiated by the helical modes, we consider the radial structure of T_{xx}, modelling it as

$$T_{xx}(x, r, m, \omega) = 2\rho_0 \bar{u}_x(r)\, \hat{u}_x(r, m, \omega) \mathrm{e}^{-\mathrm{i}kx} \mathrm{e}^{-x^2/L^2}, \tag{5.2}$$

where $\bar{u}_x(r)$ was taken as the mean velocity profile at $x = D$, and the velocity fluctuations $\hat{u}_x(r, m, \omega)$ were modelled as linear instability waves of frequency ω and azimuthal mode m. A linear spatial stability analysis is performed, based on a parallel shear flow whose mean velocity profile is that measured at $x = D$, and the most unstable mode used in order to model the radial structure of the source. Radial distributions of velocity fluctuations obtained in this way have previously been seen to closely match experimental results for forced jets (Cohen & Wygnanski 1987; Petersen & Samet 1988), and there is evidence of similar agreement of instability wave models for unforced jets (Gudmundsson & Colonius 2011).

The linear spatial instability calculation was performed assuming parallel, compressible, inviscid flow, as in Michalke (1984). Numerical results were obtained with a Runge–Kutta integration in a shooting procedure, and the present results were seen to reproduce growth rates and convection velocities of the cited paper. Radial eigenfunctions so obtained are shown in figure 21. The eigenfunctions have a near-zero amplitude close to the jet lipline. This low amplitude is seen in figure 21(*b*) to correspond to a position where the phase has an jump of π. The two sides of the jet mixing layer present a phase opposition for the axial velocity, a feature observed in

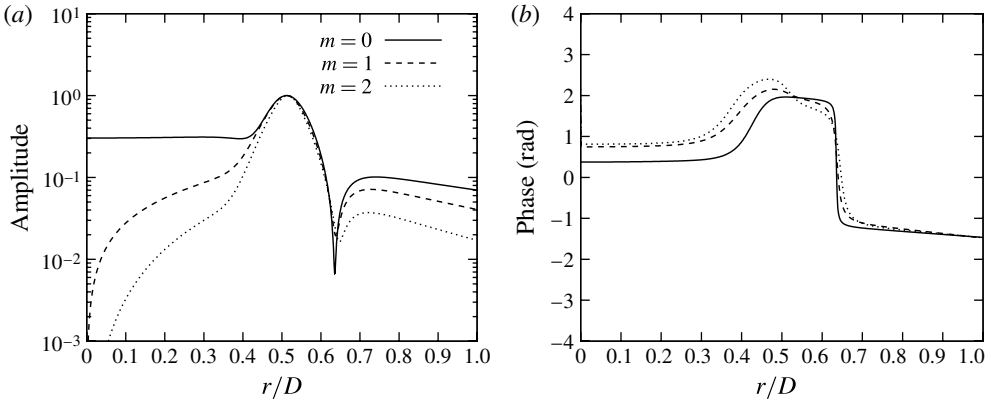

FIGURE 21. Axial velocity of eigenfunctions obtained with linear stability theory for $x = D$ and $St = 0.2$: (*a*) amplitude and (*b*) phase.

Azimuthal mode	U_c/U	kL
0	0.97	6.0
1	0.72	3.3
2	0.63	2.3

TABLE 6. Wavepacket parameters for $M = 0.6$ and $St = 0.2$.

forced jets (Cohen & Wygnanski 1987; Petersen & Samet 1988), but also in natural, turbulent jets (Lau, Fisher & Fuchs 1972).

The source defined in (5.2) was used in (5.1) to obtain the radiated sound field for azimuthal modes 0, 1 and 2 as

$$p(R,\theta,m,\omega) = -\frac{\mathrm{i}^m \rho_0 k_a^2 \cos^2\theta \mathrm{e}^{-\mathrm{i}k_a R}}{R} \int \exp[\mathrm{i}(k_a x\cos\theta - kx) - x^2/L^2]\,\mathrm{d}x$$
$$\times \int \bar{u}_x(r)\hat{u}_x(r,m,\omega)\mathrm{J}_m(k_a r\sin\theta) r\,\mathrm{d}r. \tag{5.3}$$

The convection wavenumber k was taken as the real part of the wavenumber predicted by the stability calculation. Equation (5.2) has two parameters: a free amplitude for $\hat{u}_x(r,m,\omega)$ and the wavepacket characteristic length L. The free amplitude was determined so as to match the SPL values at $\theta = 30°$, and L was chosen to provide the best agreement with the other angles. Results are presented in figure 22, and the wavepacket parameters summarized in table 6. The calculated sound radiation of the wavepackets closely fits the directivity shape in the experiment for the three azimuthal modes.

The determination of kL for the axisymmetric mode, which was done in § 4.2, is repeated here, and despite the difference between the convection speed assumed in § 4.2 (0.6 times the jet velocity) and the value predicted by instability theory at $x = D$ ($0.97U$) there is little change in the estimated value of kL (compare with table 2),

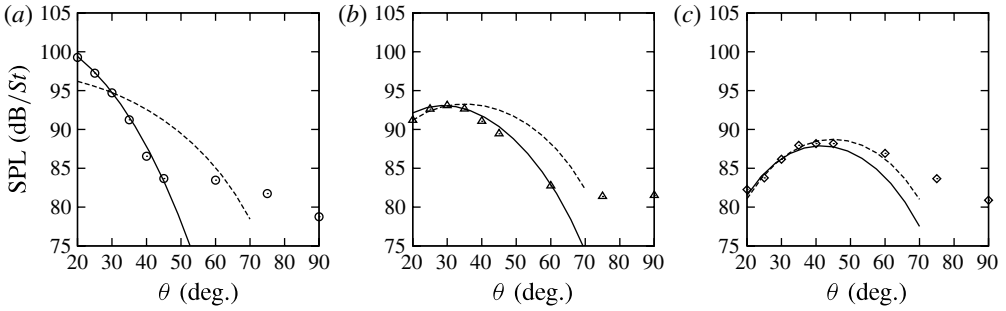

FIGURE 22. Comparison of experimental results (points) with sound radiation from wavepacket models (full lines) for $M = 0.6$, $St = 0.2$ and (*a*) $m = 0$, (*b*) $m = 1$ and (*c*) $m = 2$. Dashed lines show results assuming axial compactness ($kL \to 0$).

showing that the conclusions of § 4 do not depend on the assumption of a particular value for the convection velocity.

Figure 22 also illustrates the changes in the directivity as a function of the azimuthal mode. As m is increased, for low θ the function $\mathrm{J}_m(kr\sin\theta)$ causes a 'cut-off' of the radiated sound. This cut-off is due to the azimuthal interference in the source. In the limit $\theta = 0$ only the axisymmetric mode radiates to the far field (Michalke & Fuchs 1975), since $\mathrm{J}_m(0)$ is equal to 1 for $m = 0$ and 0 for all other m.

The azimuthal interference for the helical modes causes the sound field to lose its superdirective behaviour for higher m, with increasing cut-off with m. It is thus not surprising that superdirectivity was verified only for the axisymmetric mode, as shown in § 4. The results show however, again, that with appropriately chosen parameters the directivity shape is very closely matched by a wavepacket model.

Finally, we note that the spatial extents estimated for both helical wavepackets are significantly lower than that of the axisymmetric component. Although values of kL around 3, as in table 6 for $m = 1$, still correspond to non-compact sources (see § 3), their influence on the radiated sound is lower than for the axisymmetric mode, which may explain the Strouhal-number scaling observed in § 4.3 for $m = 1$.

To study the influence of axial non-compactness of the estimated wavepackets on the sound radiation, we have included in figure 22 dashed lines with the results for an axially compact source. We see that for $m = 0$ and $m = 1$ the axial extent of the source is significant for sound radiation, and neglect of it leads to errors in the directivity shape, particularly for the axisymmetric mode, as discussed in § 4. However, for $m = 2$ the low value of kL is such that the differences between the wavepacket model and a compact source are quite small, and axial interference does not play a significant role in this case.

Results of the sound radiation by helical wavepackets for other values of the Strouhal and Mach numbers are shown in figures 23 and 24, for azimuthal modes 1 and 2, respectively. In each calculation the radial eigenfunction of linear instability corresponding to the values of St and M was used. As before, the free amplitude of $\hat{u}_x$ is determined so as to match the radiated sound for $\theta = 30°$, and the value of L is chosen to match the directivity shape. However, we kept the same value of kL for the three Mach numbers to constrain the model, avoiding an excess of parameters to fit the experiments. The values of kL for Strouhal numbers of 0.2, 0.4 and 0.6 are shown in table 7 for azimuthal modes 1 and 2.

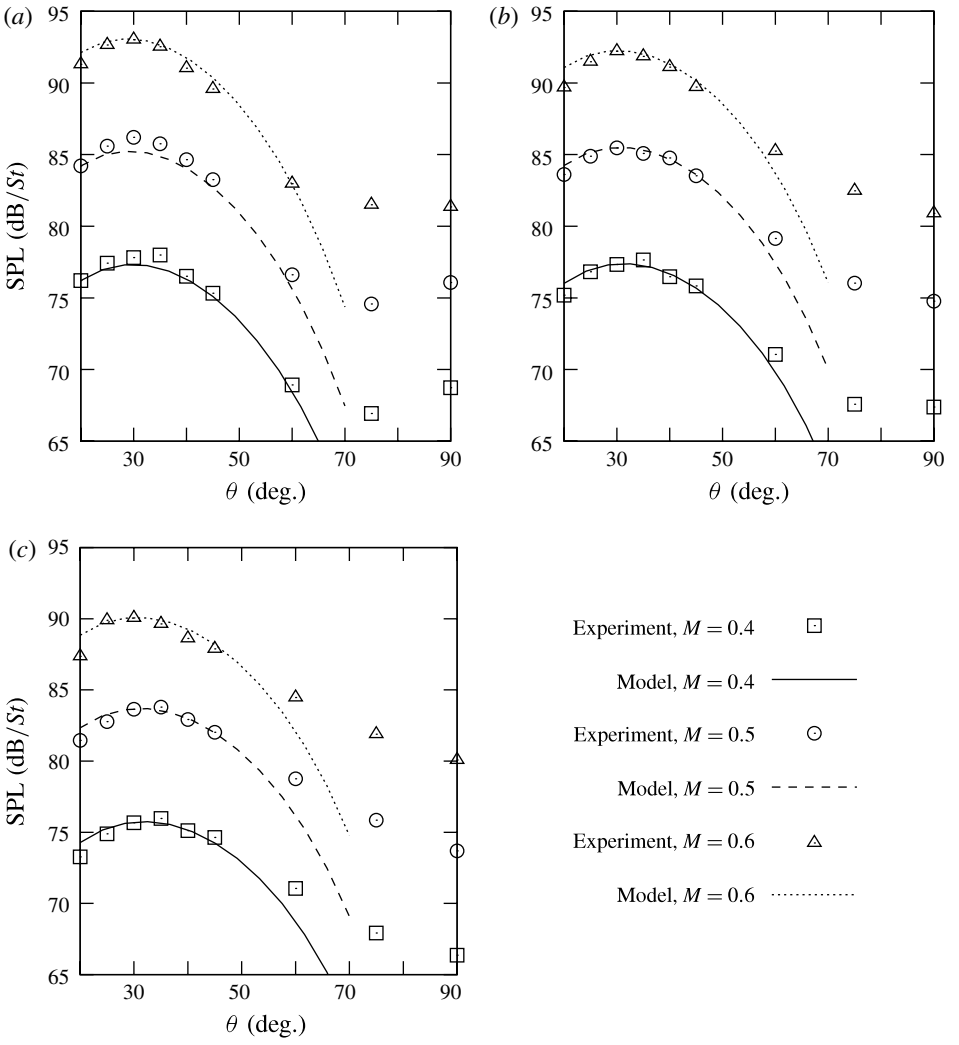

FIGURE 23. Comparison of experimental results with sound radiation from wavepacket models for azimuthal mode 1 and (*a*) $St = 0.2$, (*b*) $St = 0.4$ and (*c*) $St = 0.6$.

Azimuthal mode	$kL(St = 0.2)$	$kL(St = 0.4)$	$kL(St = 0.6)$
1	3.3	2.8	2.6
2	2.3	2.1	1.9

TABLE 7. Wavepacket parameters for the three Mach numbers in figures 23 and 24.

The results in figures 23 and 24 are close to the experimental results and present the same trends of the measurements. This confirms that the sound radiation at low angles for a range of Strouhal and Mach numbers has the directivity of helical wavepackets.

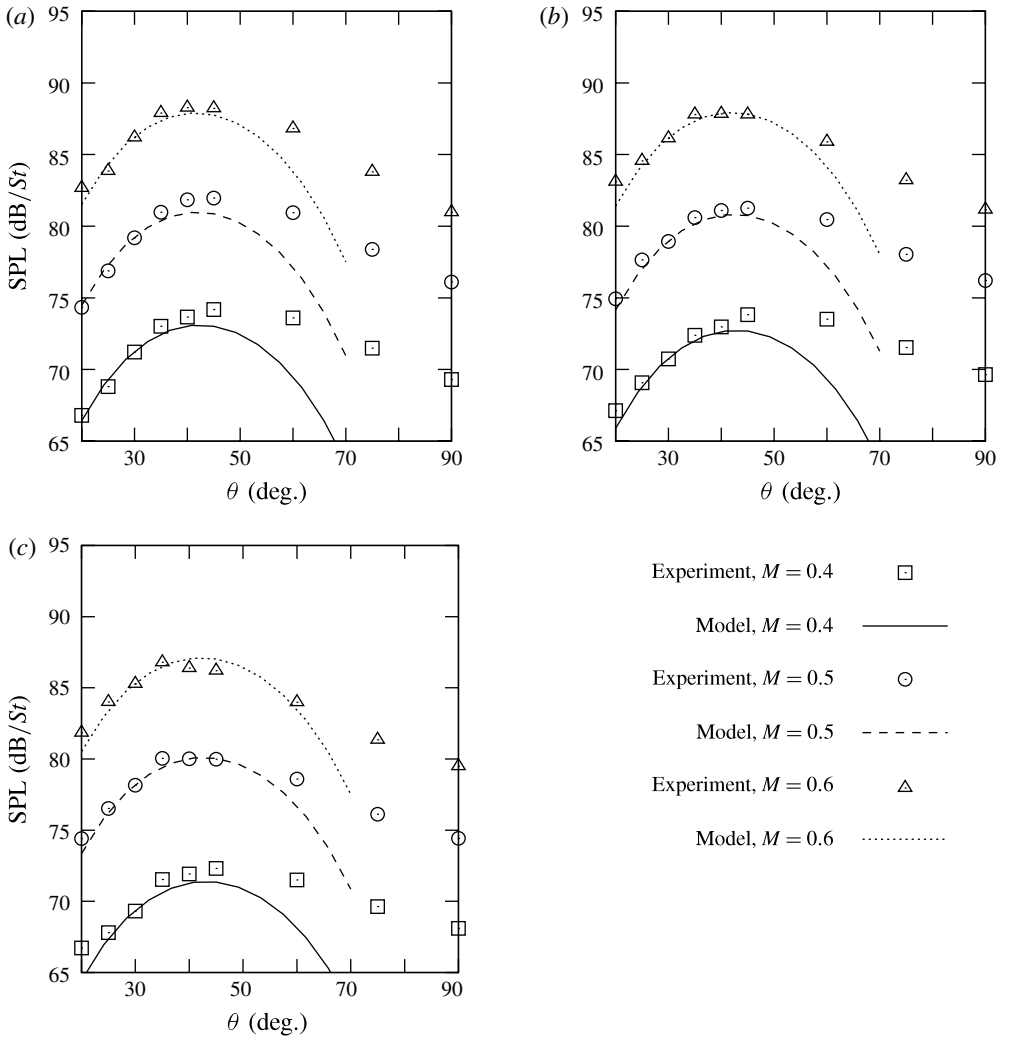

FIGURE 24. Comparison of experimental results with sound radiation from wavepacket models for azimuthal mode 2 and (*a*) $St = 0.2$, (*b*) $St = 0.4$ and (*c*) $St = 0.6$.

6. Conclusion

An experimental investigation of the azimuthal components of the sound radiated by subsonic jets in the Mach number range $0.35 \leqslant M \leqslant 0.6$ has been carried out using a ring array comprising six microphones. For this Mach-number range the axisymmetric mode is seen to be highly directive, large increases in intensity being observed as the angle to the downstream jet axis is decreased. This trend is more marked for the peak frequencies. The observed increase is such that the axisymmetric mode dominates the sound radiation for low polar angles.

An exponential change of SPL with the parameter $(1 - M_c \cos\theta)^2$ is predicted by wavepacket models, using an axially non-compact source distribution. The non-compactness leads to interference between different regions of the source; the sound radiation is, as a result, concentrated at low angles, and, for subsonic convection

velocities, decreases exponentially as $(1 - M_c \cos\theta)^2$ is increased. This effect has been observed for the axisymmetric mode, a decay of 15.4 dB being seen for the peak frequency. With this value, and a wavepacket *Ansatz*, the axial extent of the source has been estimated to be of the order of 6–8 jet diameters for the $M = 0.4$, 0.5 and 0.6 jets. Further evidence of the importance of the non-compactness of the source for the axisymmetric mode is observed in a Helmholtz scaling of the axisymmetric mode and in a velocity dependence with an exponent of 9.6 for low angles.

The analysis is extended to include higher-order azimuthal modes, and a model is proposed for sound radiation to low polar angles by helical wavepackets. The superdirective radiation, characteristic of the axisymmetric mode, is changed due to the azimuthal interference in the source, which reduces the radiation for low θ. The model presents favourable comparisons with measurements for modes 1 and 2, showing that the sound field for helical modes also corresponds to wavepacket radiation. However, the educed source extents are decreased for higher azimuthal modes, and, for mode 2, are close to the compact limit.

Since the present Mach-number range is below most aeronautical applications, it is useful to evaluate the trends with increasing M. Recalling that the velocity exponent n in (4.1) and (4.2) and in figure 18 reflects the increment of the radiated sound as M is increased, the observations in the present work allow the following scenario to be postulated with regard to the effect of increasing jet Mach number on the radiated sound.

(*a*) As the jet Mach number is increased, the sound radiation of the axisymmetric mode grows faster than the sound field of the higher-order modes (figure 18*a*).

(*b*) The increase in the axisymmetric radiation is even more pronounced near the spectral peak (figure 18*b*).

(*c*) The velocity increase therefore causes the sound radiation at low angles to be dominated by the axisymmetric mode, especially at the peak Strouhal number.

These trends suggest that at higher subsonic Mach numbers the observed axisymmetric radiation will have increased importance. Furthermore, the results suggest that the axisymmetric radiation can be appropriately modelled if, instead of considering the turbulent field to be formed by stochastic eddies with random phase (Lee & Ribner 1972; Crighton 1975), the axial interference over a non-compact source region is taken into account (see for instance Michalke 1970; Michel 2009). Some of the shortcomings in acoustic analogies may be overcome if we use appropriate source models for the large-scale structures in jets, accounting for axially extended wavepackets such as we have studied here.

For modelling purposes, we can think of the axial source interference in two ways, which are not mutually exclusive. The first is in an average sense: we look for an averaged mutual interference between the different positions of a jet, and particularly for its average effect in the sound field. For this evaluation, correlations and cross-spectra are appropriate measures, and, especially in the near field, as shown by Tinney & Jordan (2008) and Reba *et al.* (2010), these prove to be significant over a region extending several jet diameters from the nozzle exit. Furthermore, since for many practical applications determination of the radiated spectra is sufficient, this can be accomplished by coupling such correlation data with an acoustic analogy, as done, for example, by Karabasov *et al.* (2010), among others, or with a Kirchhoff surface, as shown by Reba *et al.* (2010). For such an approach, stability calculations may constitute an appropriate dynamic model, and indeed it has been shown that reasonable

predictions can be obtained for the radiated sound at low angles (Colonius, Samanta & Gudmundsson 2010).

A second approach for studying such source interference effects involves an instantaneous perspective. Since a turbulent jet is intermittent, source interference changes with time. This leads to periods when the interference is destructive, during which we have periods of 'relative quiet'; or periods during which the destructive interference may be less significant, resulting in high-energy temporally localized bursts in the acoustic field (Hileman *et al.* 2005; Kœnig *et al.* 2010). Experimental evaluation of the instantaneous interference between coherent structures in a flow is not an easy task, but such endeavours appear worthwhile considering the additional physical insight to be gained in terms of the dynamic law of jet noise source mechanisms. Furthermore, as seen by Cavalieri *et al.* (2010), the details of the mutual interference in the source region can be crucial for the understanding of differences between uncontrolled, noisy flows and their controlled, quieter counterparts.

Acknowledgements

This work was partially supported by CNPq, National Council of Scientific and Technological Development – Brazil, and through the EU–Russian program ORINOCO (FP7-AAT-2010-RTD-Russia; project number 266103). The authors thank J. Delville and C. Fourment-Cazenave for their work during the experiments.

Appendix A. Azimuthal decomposition of the acoustic field

A.1. *Definitions*

We present here the azimuthal Fourier series applied for the far-field pressure. The coefficients of a Fourier series in Φ are given by

$$p(R,\theta,m,t)=\frac{1}{2\pi}\int_{-\pi}^{\pi}p(R,\theta,\Phi,t)\mathrm{e}^{\mathrm{i}m\Phi}\,\mathrm{d}\Phi, \tag{A 1}$$

and the reconstruction of the pressure signal is

$$p(R,\theta,\Phi,t)=\sum_{m=-\infty}^{\infty}p(R,\theta,m,t)\mathrm{e}^{-\mathrm{i}m\Phi} \tag{A 2}$$

with the property

$$p(R,\theta,-m,t)=p^{*}(R,\theta,m,t) \tag{A 3}$$

since the pressure is a real-valued function.

In particular, we have for $\Phi=0$ the reconstruction

$$p(R,\theta,\Phi=0,t)=\sum_{m=-\infty}^{\infty}p(R,\theta,m,t), \tag{A 4}$$

and each azimuthal component is given by

$$p_0(R,\theta,\Phi=0,t)=p(R,\theta,m=0,t), \tag{A 5}$$

$$p_m(R,\theta,\Phi=0,t)=p(R,\theta,m,t)+p(R,\theta,-m,t)\quad\text{if } m\neq 0. \tag{A 6}$$

The azimuthal components p_m so defined are real-valued. The use of $\Phi=0$ for the reconstruction is without loss of generality due to the circumferential homogeneity of the acoustic field of axisymmetric jets.

A.2. *Evaluation of the accuracy of the Fourier series*

In the present work we have used a ring of six microphones in the far field to determine the azimuthal Fourier modes of the acoustic pressure. In order to evaluate if the spacing of $\varphi = 60°$ between microphones is appropriate, we evaluate the coherence function

$$C(\varphi, \omega) = \frac{|W(\varphi, \omega)|^2}{S_{pp}(\Phi_0, \omega) S_{pp}(\Phi_0 + \varphi, \omega)} \tag{A 7}$$

where S_{pp} is the power spectral density of a single microphone and W is the cross-spectral density between two microphones spaced azimuthally by φ, given as

$$W(\varphi, \omega) = \hat{p}(\Phi, \omega)\hat{p}^*(\Phi + \varphi, \omega), \tag{A 8}$$

where averaging between Fourier transforms of segments of the time series is implicit, and the spherical coordinates R and θ have been dropped for compactness.

The relationship between the coherence function and the azimuthal Fourier series can be obtained as follows. Using (A 2), the spatio-temporal correlation of two microphones spaced by φ with a time lag of τ can be written as

$$p(\Phi, t)p(\Phi + \varphi, t + \tau) = \sum_{m=0}^{\infty} p_m(t)p_m(t + \tau)\cos(m\varphi) \tag{A 9}$$

since the correlation function is even in φ and does not depend on Φ due to the circumferential homogeneity of the jet.

We take the temporal average of both sides and use the correlation theorem to obtain

$$\hat{p}(\Phi, \omega)\hat{p}^*(\Phi + \varphi, \omega) = \sum_{m=0}^{\infty} |\hat{p}_m(\omega)|^2 \cos(m\varphi) \tag{A 10}$$

such that $\hat{p}_m(\omega)$ can be obtained by the cross-spectral density as

$$|\hat{p}_0(\omega)|^2 = \frac{1}{2\pi} \int_0^{2\pi} \hat{p}(\Phi, \omega)\hat{p}^*(\Phi + \varphi, \omega)\, \mathrm{d}\varphi, \tag{A 11}$$

$$|\hat{p}_m(\omega)|^2 = \frac{1}{\pi} \int_0^{2\pi} \hat{p}(\Phi, \omega)\hat{p}^*(\Phi + \varphi, \omega)\cos(m\varphi)\, \mathrm{d}\varphi \quad \text{if } m \neq 0. \tag{A 12}$$

Now consider that the integral is calculated numerically; for instance, (A 12) is approximated as

$$|\hat{p}_m(\omega)|^2 = \frac{1}{2\pi} \sum_{\varphi} \hat{p}(\Phi, \omega)\hat{p}^*(\Phi + \varphi, \omega)\cos(m\varphi)\Delta\varphi. \tag{A 13}$$

If the coherence function is zero for all but $\varphi = 0$ for some frequency ω, the microphone spacing is smaller than the azimuthal coherence length. In this case, the result will be

$$|\hat{p}_0(\omega)|^2 = \frac{1}{2\pi} |\hat{p}(\Phi, \omega)|^2 \Delta\varphi \tag{A 14}$$

and

$$|\hat{p}_m(\omega)|^2 = \frac{1}{\pi} |\hat{p}(\Phi, \omega)|^2 \Delta\varphi \quad \text{if } m \neq 0 \tag{A 15}$$

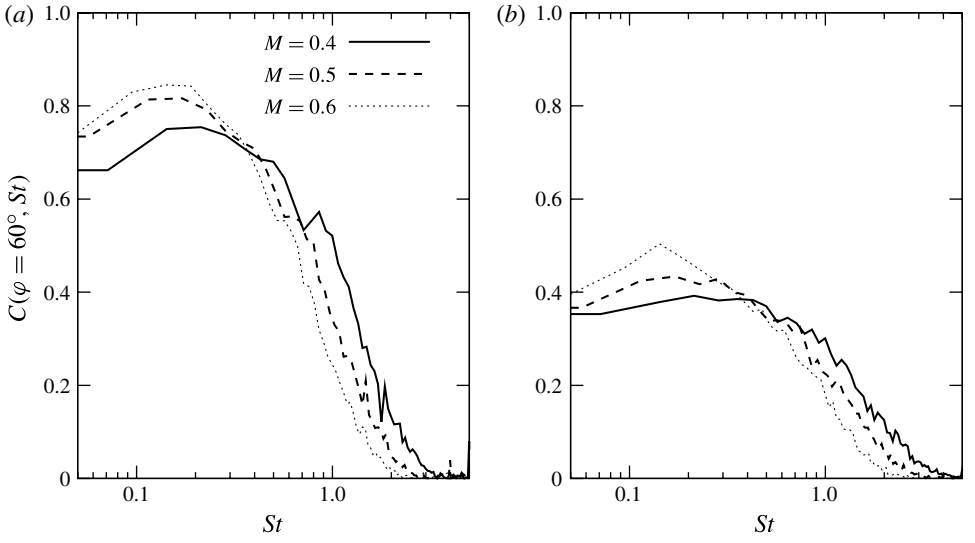

FIGURE 25. Coherence between microphones with azimuthal spacing of $\varphi = 60°$ for (*a*) $\theta = 20°$ and (*b*) $\theta = 30°$.

for all m, which is not an accurate result: a uniform distribution in azimuthal modes is obtained only for a function with zero azimuthal coherence length, but for all physical quantities this length will be finite. This result is only an artifact of the azimuthal spacing. Hence, to obtain meaningful results for the azimuthal Fourier series, the coherence should be non-zero for the microphone spacing φ.

Coherence results are shown in figure 25 for $\theta = 20°$ and $30°$. We see that for both polar angles the coherences are significant for Strouhal numbers up to 1, and decay to zero for $St \approx 2$. This validates the analysis in §§ 4 and 5, done mostly for Strouhal numbers lower than unity. However, care should be taken in analysing higher frequencies, which we avoid in the present work. For such a task an azimuthal ring with a larger number of microphones would be necessary.

Appendix B. The line-source approximation for low-angle radiation

The purpose of the present Appendix is to show, using Lighthill's analogy, the steps that allow the solution of the radiated sound at low polar angles to be expressed, in certain cases, as the radiation by a line source, such as the Crow's model in (3.6).

The solution of Lighthill's equation for the pressure p in the frequency domain is given in $\boldsymbol{x}$ as

$$p(\boldsymbol{x}, \omega) = \iiint \frac{\partial^2 T_{ij}}{\partial y_i \partial y_j}(\boldsymbol{y}, \omega) \frac{\exp(-\mathrm{i}k_a|\boldsymbol{x} - \boldsymbol{y}|)}{4\pi|\boldsymbol{x} - \boldsymbol{y}|} \,\mathrm{d}\boldsymbol{y}, \tag{B 1}$$

where $k_a = \omega/c$ is the acoustic wavenumber and a time factor of $\exp(\mathrm{i}\omega t)$ is implied.

If we are interested in the radiation to low polar angles, we can consider the T_{11} term of Lighthill's tensor alone as a first approximation. It can be shown that only the quadrupoles aligned with the radiation direction generate sound in the far acoustic field (Crighton 1975), and for low angles these quadrupoles can be approximated by the T_{11} term. Another reason is that while the velocity fluctuations in the three directions

have similar amplitudes in a jet, the mean streamwise velocity is more than an order of magnitude higher than the transverse components. The use of T_{11} alone to calculate sound radiation for low angles was used in the models of Cavalieri *et al.* (2011*b*), and led to good agreement with results of a large-eddy simulation.

We rewrite the source in cylindrical coordinates (x, r, ϕ) and the observer in spherical coordinates (R, θ, Φ). The far-field approximation gives a distance between source and observer equal to $R - x\cos\theta - r\sin\theta\cos(\phi - \Phi)$, leading to

$$p(R,\theta,\Phi,\omega) = \frac{1}{4\pi R}\iiint \frac{\partial^2 T_{xx}}{\partial x^2}(x,r,\phi,\omega) \times \exp[-\mathrm{i}k_a(R - x\cos\theta - r\sin\theta\cos(\phi-\Phi))]r\,\mathrm{d}x\,\mathrm{d}r\,\mathrm{d}\phi. \quad (B\,2)$$

The double derivative can be passed from Lighthill's tensor to the Green's function, as shown, for instance, by Goldstein (1976). This gives

$$p(R,\theta,\Phi,\omega) = \frac{1}{4\pi R}\iiint T_{xx}(x,r,\phi,\omega) \times \frac{\partial^2}{\partial x^2}[\exp[-\mathrm{i}k_a(R - x\cos\theta - r\sin\theta\cos(\phi-\Phi))]]r\,\mathrm{d}x\,\mathrm{d}r\,\mathrm{d}\phi. \quad (B\,3)$$

The azimuthal dependence of T_{xx} can be expanded in an azimuthal Fourier series. Taking the mode m of T_{xx} leads to

$$p(R,\theta,\Phi,\omega) = \frac{1}{4\pi R}\iiint T_{xx}(x,r,m,\omega)\mathrm{e}^{-\mathrm{i}m\phi} \times \frac{\partial^2}{\partial x^2}[\exp[-\mathrm{i}k_a(R - x\cos\theta - r\sin\theta\cos(\phi-\Phi))]]r\,\mathrm{d}x\,\mathrm{d}r\,\mathrm{d}\phi, \quad (B\,4)$$

which can be manipulated to give

$$p(R,\theta,\Phi,\omega) = \frac{\mathrm{e}^{-\mathrm{i}m\Phi}}{4\pi R}\iiint T_{xx}(x,r,m,\omega)\mathrm{e}^{-\mathrm{i}m(\phi-\Phi)} \times \frac{\partial^2}{\partial x^2}[\exp[-\mathrm{i}k_a(R - x\cos\theta - r\sin\theta\cos(\phi-\Phi))]]r\,\mathrm{d}x\,\mathrm{d}r\,\mathrm{d}\phi. \quad (B\,5)$$

Integration in cylindrical coordinates gives

$$p(R,\theta,\Phi,\omega) = \mathrm{e}^{-\mathrm{i}m\Phi}\frac{\mathrm{e}^{-\mathrm{i}k_aR}}{4\pi R}\int \mathrm{d}x\int T_{xx}(x,r,m,\omega)\frac{\partial^2}{\partial x^2}[\mathrm{e}^{\mathrm{i}(k_ax\cos\theta)}]r\,\mathrm{d}r \times \int \mathrm{e}^{-\mathrm{i}m(\phi-\Phi)}\exp[\mathrm{i}k_ar\sin\theta\cos(\phi-\Phi)]\,\mathrm{d}\phi. \quad (B\,6)$$

From the integral representation of the Bessel functions J_m with integer m (Morse & Ingard 1968)

$$\mathrm{J}_m(x) = \frac{1}{2\pi\mathrm{i}^m}\int_0^{2\pi}\mathrm{e}^{\mathrm{i}x\cos\phi}\cos(m\phi)\,\mathrm{d}\phi, \quad (B\,7)$$

we can deduce the azimuthal integral to be equal to $2\pi\mathrm{i}^m\mathrm{J}_m(k_ar\sin\theta)$. This leads to

$$p(R,\theta,\Phi,\omega) = -\mathrm{e}^{-\mathrm{i}m\Phi}\frac{\mathrm{i}^m k_a^2\cos^2\theta\mathrm{e}^{-\mathrm{i}k_aR}}{2R}\int \mathrm{e}^{\mathrm{i}k_ax\cos\theta}\,\mathrm{d}x\int T_{xx}(x,r,m,\omega) \times \mathrm{J}_m(k_ar\sin\theta)r\,\mathrm{d}r. \quad (B\,8)$$

In (B 8) we see that an azimuthal mode m of T_{xx} leads to an $\mathrm{e}^{-\mathrm{i}m\Phi}$ factor in the radiated pressure, showing that there is a direct correspondence between the azimuthal modes in the source and in the acoustic field, such that

$$p(R,\theta,m,\omega) = -\frac{\mathrm{i}^m k_a^2 \cos^2\theta \mathrm{e}^{-\mathrm{i}k_a R}}{2R} \int \mathrm{e}^{\mathrm{i}k_a x\cos\theta}\,\mathrm{d}x \int T_{xx}(x,r,m,\omega) \times \mathrm{J}_m(k_a r\sin\theta) r\,\mathrm{d}r \qquad \text{(B 9)}$$

where $p(R,\theta,m,\omega)$ is the coefficient of azimuthal mode m of the radiated pressure.

For the axisymmetric mode, (B 9) gives

$$p(R,\theta,m=0,\omega) = -\frac{k_a^2 \cos^2\theta \mathrm{e}^{-\mathrm{i}k_a R}}{2R} \int \mathrm{e}^{\mathrm{i}k_a x\cos\theta}\,\mathrm{d}x \int T_{xx}(x,r,m=0,\omega) \times \mathrm{J}_0(k_a r\sin\theta) r\,\mathrm{d}r. \qquad \text{(B 10)}$$

If $k_a r\sin\theta \ll 1$, we can make a further approximation by taking $\mathrm{J}_0(k_a r\sin\theta)$ to be 1 (more precisely, since $\mathrm{J}_0(x) \approx 1 - x^2/4$ for small x, the approximation of $\mathrm{J}_0(k_a r\sin\theta)$ as 1 is reasonable if $k_a^2 r^2 \sin^2\theta/4 \ll 1$). Noting that

$$k_a r\sin\theta = 2\pi St M \frac{r}{D}\sin\theta \qquad \text{(B 11)}$$

and considering that the radial integration in (B 8) has significant values for values of r not much larger than D, the approximation of $\mathrm{J}_0(k_a r\sin\theta)$ as 1 is reasonable for low values of the radiation angle and of the Strouhal and Mach numbers.

The far-field pressure is then given as

$$p(R,\theta,m=0,\omega) = -\frac{k_a^2 \cos^2\theta \mathrm{e}^{-\mathrm{i}k_a R}}{2R} \int \mathrm{e}^{\mathrm{i}k_a x\cos\theta}\mathrm{d}x \int T_{xx}(z,r,m=0,\omega) r\,\mathrm{d}r, \qquad \text{(B 12)}$$

and the axisymmetric source can be approximated as a line distribution of quadrupoles with intensity

$$S_{xx}(x,m=0,\omega) = \int T_{xx}(x,r,m=0,\omega) r\,\mathrm{d}r. \qquad \text{(B 13)}$$

This or similar approximations have been used in a number of works in the literature (Crow 1972; Ffowcs Williams & Kempton 1978; Cavalieri *et al.* 2011*b*). The far-field pressure is given as

$$p(R,\theta,m=0,\omega) = -\frac{k_a^2 \cos^2\theta \mathrm{e}^{-\mathrm{i}k_a R}}{2R} \int S_{xx}(x,m=0,\omega)\mathrm{e}^{-\mathrm{i}k_a x\cos\theta}\,\mathrm{d}x. \qquad \text{(B 14)}$$

REFERENCES

ARMSTRONG, R. R., FUCHS, H. V. & MICHALKE, A. 1977 Coherent structures in jet turbulence and noise. *AIAA J.* **15**, 1011–1017.

BATCHELOR, G. K. & GILL, A. E. 1962 Analysis of the stability of axisymmetric jets. *J. Fluid Mech.* **14** (4), 529–551.

BOGEY, C., BARRÉ, S., FLEURY, V., BAILLY, C. & JUVÉ, D. 2007 Experimental study of the spectral properties of near-field and far-field jet noise. *Intl J. Aeroacoust.* **6** (2), 73–92.

BRIDGES, J. E. & HUSSAIN, A. K. M. F. 1987 Roles of initial condition and vortex pairing in jet noise. *J. Sound Vib.* **117** (2), 289–311.

BROWN, C. A. & BRIDGES, J. 2006 Acoustic efficiency of azimuthal modes in jet noise using chevron nozzles. *Tech. Rep.* National Aeronautics and Space Administration.

CAVALIERI, A. V. G., DAVILLER, G., COMTE, P., JORDAN, P., TADMOR, G. & GERVAIS, Y. 2011*a* Using large eddy simulation to explore sound-source mechanisms in jets. *J. Sound Vib.* **330** (17), 4098–4113.

CAVALIERI, A. V. G., JORDAN, P., AGARWAL, A. & GERVAIS, Y. 2011*b* Jittering wave-packet models for subsonic jet noise. *J. Sound Vib.* **330** (18–19), 4474–4492.

CAVALIERI, A. V. G., JORDAN, P., GERVAIS, Y., WEI, M. & FREUND, J. B. 2010 Intermittent sound generation and its control in a free-shear flow. *Phys. Fluids* **22** (11), 115113.

COHEN, J. & WYGNANSKI, I. 1987 The evolution of instabilities in the axisymmetric jet. Part 1. The linear growth of disturbances near the nozzle. *J. Fluid Mech.* **176**, 191–219.

COLONIUS, T., SAMANTA, A. & GUDMUNDSSON, K. 2010 Parabolized stability equation models of large-scale jet mixing noise. *Procedia Engng* **6**, 64–73.

CRIGHTON, D. G. 1975 Basic principles of aerodynamic noise generation. *Prog. Aerosp. Sci.* **16** (1), 31–96.

CRIGHTON, D. G. & GASTER, M. 1976 Stability of slowly diverging jet flow. *J. Fluid Mech.* **77** (2), 397–413.

CRIGHTON, D. G. & HUERRE, P. 1990 Shear-layer pressure fluctuations and superdirective acoustic sources. *J. Fluid Mech.* **220**, 355–368.

CROW, S. C. 1972 Acoustic gain of a turbulent jet. In *Paper IE.6, Meeting of Division of Fluid Dynamics, American Physical Society, University of Colorado, Boulder, November 1972*.

CROW, S. C. & CHAMPAGNE, F. H. 1971 Orderly structure in jet turbulence. *J. Fluid Mech.* **48** (3), 547–591.

FFOWCS WILLIAMS, J. E. & KEMPTON, A. J. 1978 The noise from the large-scale structure of a jet. *J. Fluid Mech.* **84** (4), 673–694.

FUCHS, H. V. & ARMSTRONG, R. R. 1978 Turbulent source coherence and Helmholtz number as aerodynamic noise parameters. In *Structure and Mechansims of Turbulence* (ed. H. Fiedler). vol. II. pp. 189–201. Springer.

FUCHS, H. V. & MICHEL, U. 1978 Experimental evidence of turbulent source coherence affecting jet noise. *AIAA J.* **16** (9), 871–872.

GOLDSTEIN, M. E. 1976 *Aeroacoustics*, p. 305. McGraw-Hill.

GUDMUNDSSON, K. & COLONIUS, T. 2011 Instability wave models for the near-field fluctuations of turbulent jets. *J. Fluid Mech.* **689**, 97–128.

HILEMAN, J. I., THUROW, B. S., CARABALLO, E. J. & SAMIMY, M. 2005 Large-scale structure evolution and sound emission in high-speed jets: real-time visualization with simultaneous acoustic measurements. *J. Fluid Mech.* **544**, 277–307.

HUSSAIN, A. K. M. F. & ZAMAN, K. B. M. Q. 1981 The 'preferred mode' of the axisymmetric jet. *J. Fluid Mech.* **110**, 39–71.

JUVÉ, D., SUNYACH, M. & COMTE-BELLOT, G. 1979 Filtered azimuthal correlations in the acoustic far field of a subsonic jet. *AIAA J.* **17**, 112.

KARABASOV, S., AFSAR, M. Z., HYNES, T. P., DOWLING, A. P., MCMULLAN, W. A., POKORA, C. D., PAGE, G. J. & MCGUIRK, J. J. 2010 Jet noise: acoustic analogy informed by large eddy simulation. *AIAA J.* **48** (7), 1312–1325.

KŒNIG, M., CAVALIERI, A. V. G., JORDAN, P., DELVILLE, J., GERVAIS, Y., PAPAMOSCHOU, D., SAMIMY, M. & LELE, S. K. 2010 Farfield pre-filterering and source-imaging for the study of jet noise. In *16th AIAA/CEAS Aeroacoustics Conference and Exhibit*. Stockholm, Sweden.

LAU, J. C., FISHER, M. J. & FUCHS, H. V. 1972 The intrinsic structure of turbulent jets. *J. Sound Vib.* **22** (4), 379–384.

LAUFER, J. & YEN, T.-C. 1983 Noise generation by a low-Mach-number jet. *J. Fluid Mech.* **134**, 1–31.

LEE, H. K. & RIBNER, H. S. 1972 Direct correlation of noise and flow of a jet. *J. Acoust. Soc. Am.* **52**, 1280.

LELE, S. K. 1994 Compressibility effects on turbulence. *Annu. Rev. Fluid Mech.* **26** (1), 211–254.

LIGHTHILL, M. J. 1952 On sound generated aerodynamically. I. General theory. *Proc. R. Soc. Lond.* A **211** (1107), 564–587.

LUSH, P. A. 1971 Measurements of subsonic jet noise and comparison with theory. *J. Fluid Mech.* **46** (3), 477–500.

MANKBADI, R. & LIU, J. T. C. 1984 Sound generated aerodynamically revisited: large-scale structures in a turbulent jet as a source of sound. *Phil. Trans. R. Soc. Lond.* A **311** (1516), 183–217.

MICHALKE, A. 1970 A wave model for sound generation in circular jets. *Tech. Rep.* Deutsche Luft- und Raumfahrt.

MICHALKE, A. 1971 Instabilitat eines Kompressiblen Runden Freistrahls unter Berucksichtigung des Einflusses der Strahlgrenzschichtdicke. *Z. Flugwiss.* **19**, 319–328; English translation: *NASA TM 75190, 1977.*

MICHALKE, A. 1972 An expansion scheme for the noise from circular jets. *Z. Flugwiss.* **20**, 229–237.

MICHALKE, A. 1984 Survey on jet instability theory. *Prog. Aerosp. Sci.* **21**, 159–199.

MICHALKE, A. & FUCHS, H. V. 1975 On turbulence and noise of an axisymmetric shear flow. *J. Fluid Mech.* **70**, 179–205.

MICHEL, U. 2009 The role of source interference in jet noise. In *15th AIAA/CEAS Aeroacoustics Conference (30th Aeroacoustics Conference)*, pp. 1–15.

MOLLO-CHRISTENSEN, E. 1963 Measurements of near field pressure of subsonic jets. *Tech. Rep.* Advisory Group for Aeronautical Research and Development, Paris, France.

MOLLO-CHRISTENSEN, E. 1967 Jet noise and shear flow instability seen from an experimenter's viewpoint (Similarity laws for jet noise and shear flow instability as suggested by experiments). *Trans. ASME: J. Appl. Mech.* **34**, 1–7.

MOORE, C. J. 1977 The role of shear-layer instability waves in jet exhaust noise. *J. Fluid Mech.* **80** (2), 321–367.

MORRIS, P. J. 2010 The instability of high speed jets. *Intl J. Aeroacoust.* **9** (1), 1–50.

MORSE, P. M. & INGARD, K. U. 1968 *Theoretical Acoustics*. McGraw-Hill.

PETERSEN, R. A. & SAMET, M. M. 1988 On the preferred mode of jet instability. *J. Fluid Mech.* **194**, 153–173.

REBA, R., NARAYANAN, S. & COLONIUS, T. 2010 Wave-packet models for large-scale mixing noise. *Intl J. Aeroacoust.* **9** (4), 533–558.

SANDHAM, N. D., MORFEY, C. L. & HU, Z. W. 2006 Sound radiation from exponentially growing and decaying surface waves. *J. Sound Vib.* **294** (1), 355–361.

SUZUKI, T. & COLONIUS, T. 2006 Instability waves in a subsonic round jet detected using a near-field phased microphone array. *J. Fluid Mech.* **565**, 197–226.

TANNA, H. K. 1977 An experimental study of jet noise. Part I. Turbulent mixing noise. *J. Sound Vib.* **50** (3), 405–428.

TINNEY, C. E. & JORDAN, P. 2008 The near pressure field of co-axial subsonic jets. *J. Fluid Mech.* **611**, 175–204.

TUTKUN, M., GEORGE, W. K., FOUCAUT, J. M., COUDERT, S., STANISLAS, M. & DELVILLE, J. 2009 In situ calibration of hot wire probes in turbulent flows. *Exp. Fluids* **46** (4), 617–629.

VISWANATHAN, K. 2004 Aeroacoustics of hot jets. *J. Fluid Mech.* **516**, 39–82.

VISWANATHAN, K. 2006 Scaling laws and a method for identifying components of jet noise. *AIAA J.* **44** (10), 2274.

ZAMAN, K. B. M. Q. & YU, J. C. 1985 Power spectral density of subsonic jet noise. *J. Sound Vib.* **98** (4), 519–537.